Journal of Asian Earth Sciences 185 (2019) 104023

Contents lists available at ScienceDirect

Journal of Asian Earth Sciences

journal homepage: www.elsevier.com/locate/jseaes

Behaviors of REEs during pedogenetic processes in the karst areas of Southwest China

Cheng Chang[a], Changshun Song[b,c], Howard Omar Beckford[a], Shijie Wang[b], Hongbing Ji[a,b,*]

[a] School of Energy and Environmental Engineering, University of Science and Technology Beijing, Beijing 100083, China
[b] State Key Laboratory of Environmental Geochemistry, Institute of Geochemistry, Chinese Academy of Sciences, Guiyang 550002, China
[c] University of the Chinese Academy of Sciences, Beijing 100049, China

ARTICLE INFO

Keywords:
Weathering profile
Rare earth elements
Leaching
Ce anomaly
Guizhou

ABSTRACT

To understand the behavior of rare earth elements (REEs) during pedogenetic processes in karst area, SW China, we investigated the leaching characteristics in order to better understand the mobility and fractionation of REEs in two soil profiles developed on dolomite. The two soil profiles, namely, Qingzhen (QZ) and Pingba (PB), were sampled from Guizhou province. Hydrochloric acid leaching method was used, and the soil samples from the profiles were compared. REE contents decreased from the bottom of the profiles (1360.39 ppm of QZ and 2236.61 ppm of PB) to the topsoil (247.32 ppm of QZ and 168 ppm of PB). From the soil samples to leachates, $(La/Yb)_N$ (N means chondrite-normalized values) increased from 3–8.92 to 2.36–25.02 in QZ and 6.34–9.06 to 5.28–14.83 in PB, and $(Gd/Yb)_N$ increased from 1.01–1.80 to 1.40–2.71 in QZ and 1.16–2.03 to 2.07–3.29 in PB. These results indicate that the degree of REE fractionation increases with continuous weathering. Obvious differences in LREE/HREE and ΣREE/Th ratios between the soil samples and leachates indicated strong weathering and pedogenesis under a simulated acid leaching environment. Negative and positive cerium (Ce) anomalies were observed in the lower and upper parts, respectively, of the profiles. Ce anomalies in the soil samples and leachates may be due to the sensitivity of Ce to redox conditions. Given that the decrease of Y/Ho ratio and the negative correlation with soil pH, incipient pedogenetic processes likely play an important role in Y-Ho fractionation. On the basis of the characteristics of REE behavior, the studied profiles have the characteristics of in situ weathering.

1. Introduction

The behavior of rare earth elements (REEs) serves as a valuable indicator in the investigation of geological and biogeochemical processes, such as upper continental crust development (Braun et al., 1998; Taylor and McLennan, 1981; Taylor et al., 1986), sediment provenance (Jung et al., 2016; Ni et al., 2017; McLennan, 1989), and weathering processes (Berger et al., 2014; Ji et al., 2004a; Laveuf and Cornu, 2009; Leleyter et al., 1999). Studying the release, retention, and transport of REEs under different conditions at the Earth's surface is crucial to understanding REE behavior and tracing pedogenetic processes (Jin et al., 2017; Laveuf and Cornu, 2009). Over the past decades, considerable attention has been paid to REE fractionation and Ce anomalies in weathering environments (Boulangé and Colin, 1994; Braun et al., 1990; Nesbitt and Markovics, 1980; Öhlander et al., 1996; Vermeire et al., 2016). The following three factors have been proposed to lead to the REE fractionation process: (1) stability of primary REE-bearing minerals (Duddy, 1980; Öhlander et al., 1996), (2) difference in complexation ability with ligands between light rare earth element (LREE) and heavy rare earth element (HREE) (Braun et al., 1990; Braun et al., 2017; Leleyter et al., 1999), and (3) weathering conditions, such as redox and pH, that lead to Ce anomaly (Marsh, 1991; Mongelli, 1993).

Acid leaching is an effective method for obtaining useful information on REE behavior in weathering profiles. Nasraoui et al. (2000) revealed that the presence of REEs provides the basis for REE enrichment and mobilization by chemical sequential extraction. After conducting leaching experiments on carbonates, Ji et al. (2004b) suggested that REEs are present in clay minerals and other secondary phosphate phases. Ni et al. (2017) utilized 1 N HCl to divide samples into two phases, namely, leached and residual fractions, and suggested that Mn–Fe (hydro)oxides and secondary phosphate minerals are the main hosts of acid-leachable REE.

Redox conditions in soils from tropical and subtropical zones are different from those from temperate zones. Hence, the style of mobilization and redistribution of elements during chemical weathering are different (Hill et al., 2000; Ma et al., 2007b; Young and Nesbitt, 1998).

* Correspondence author at: University of Science and Technology Beijing, Xueyuan Road No. 30, Haidian District, Beijing 100083, China.
E-mail address: ji.hongbing@hotmail.com (H. Ji).

https://doi.org/10.1016/j.jseaes.2019.104023
Received 15 January 2019; Received in revised form 9 September 2019; Accepted 9 September 2019
Available online 10 September 2019
1367-9120/

Laterites, which are the products of chemical weathering under tropical or subtropical climate (Nahon, 2003), are widely distributed in southern China. The behavior of REEs in laterites during chemical weathering is less studied. Therefore, a comprehensive understanding of REE mobility and fractionation is important. Studying the behavior of REEs in laterites will improve understanding of weathering and pedogenesis in southern China especially in karst regions. Other main interests in the study of REE behavior under tropical and subtropical weathering are the accumulation of REEs in soil profiles and the transformation of REEs to economically valuable deposits (Li et al., 2017). Also, Li et al. (2019) studied the genesis of Zudong REE deposit in South China, and so it will be of great importance to explore similar deposits in other parts of the world.

Two weathering profiles that developed on Triassic dolomites in Guizhou Province, SW China were selected for this study. It is recognized that in carbonate rocks, REEs are contained in three fractions: the detritus fraction, the absorbed fraction and the authigenic carbonate and phosphate (Balashov and Girin, 1969; Ji et al., 2004b; Parekh et al., 1977). Hydrochloric acid leaching method was used to decipher the behaviors of REEs in the Qingzhen (QZ) and Pingba (PB) profiles. The purpose of this study is to explore REE behavior in adsorbed fractions under supergene condition, rather than the distribution of REEs in minerals during the sedimentary and diagenetic processes. Thus, 1 N HCl was used for the leaching experiment, which was found to be effective in demonstrating REE distribution and behaviors as it does not dissolve minerals in the weathering regolith, except for some soluble phosphate minerals (Ma et al., 2007a; Wang et al., 1999). REE mobilization and fractionation were described and discussed in detail by using sequence parameters and ratios in leachates and soil samples. This approach can help us understand REE migration and retention during pedogenesis in the karst region of SW China.

2. Materials and methods

2.1. Geological background and sample collection

The study area is located in the Yunnan–Guizhou Plateau. Guizhou Province has a moist climate and is located in the karst terrain in SW China (Fig. 1). This karst terrain is one of the largest continuously distributed karst landforms in the world and is extensively developed in Guizhou province. The climate in this region is subtropical monsoon, which is controlled by the East Asia summer, Indian Ocean, and Qinghai–Tibet Plateau monsoons. Annual precipitation of the study area varies from 1100 mm to 1300 mm, with the rain season in May to October, accounting for 70%–85% of the annual precipitation. The weather is relatively moderate with a mean annual temperature of above 15 °C.

The PB profile (26° 26′ N, 106° 22′ E) is located in Pingba Farm at approximately 40 km southwest of Guiyang, which is the capital of Guizhou Province. The QZ profile (26° 21′ N, 106° 31′ E) is between Pingba Farm and Guiyang. The bedrock is sedimentary dolomite and belongs to the Triassic Anshun Formation. The sampling point and area lithology are illustrated in Fig. 1. Soil profiles were established by recent road construction. Soil samples were collected from the surface downward to the bedrock through the profile. The surface comprised loose soil covered with flourishing vegetation. Beneath the surface soil was a yellow-brown fine homogeneous laterite soil, and sampling interval was about 20–25 cm (from QZ-25 to QZ-04 and PB-22 to PB-04). The QZ profile had an 8 cm-thick ferruginous crust layer between 130 and 155 cm. The soils in this layer contained some black material and the color turns into brick red. A thin layer of grayish white flour dolomite (rock powder) was present at a depth of 555 cm in the QZ profile (480 cm in the PB profile). The rock powder was sampled as QZ-03 (PB-03). Saprock and bedrock samples were collected beneath the flour dolomite layer (Fig. 2). A total of 43 soil samples were collected from both profiles (23 in QZ and 20 in PB). The soil samples were collected from bottom to top, and the numbering was as follows: QZ-01 and QZ-02 (parent rock samples) and QZ-03 (rock powder) to QZ-25 (surface soil). The same order was used for the PB profile.

Previous studies showed that the major mineral constituents of the PB profile are illite, kaolinite, gibbsite, smectite, quartz, feldspar, anatase, and iron oxides (including hematite and goethite). From the XRD analysis (Fig. 3), the major mineral constituents of QZ profile are quartz and clay minerals (illite, kaolinite, and pyrophyllite). Iron-bearing minerals (magnetite and hematite) are also present. In the upper part of the profile, the contents of quartz and clay minerals increased and decreased, respectively. The horizons recognized in the profiles were soil horizon (the top as a cultivated layer); regolith horizon, which had a dark red ferruginous crust layer in the QZ profile and a weathering front; weathering bedrock horizon; and fresh bedrock horizon.

2.2. Analytical methods

The soil samples were dried under a ventilated condition with a covered thin paper to prevent the atmospheric settlement and were passed through a 2-mm sieve. Soil pH was determined at a soil to water ratio of 1:2.5, and measurement error was less than 0.1. The air-dried samples were powdered using an agate mortar and passed through a 75-μm sieve. The powdered samples were added with 1 N HCl to destroy organic matter and were dried at 60 °C. Total organic carbon (TOC) was determined by a TOC analyzer. Powdered samples were digested in a solution of HNO_3 + HF + H_2O_2 for elemental analysis.

Powdered samples (5 g) were weighed and added with 1 N HCl at room temperature for 30 min. The acid-soluble and acid-insoluble fractions were separated by centrifugation. The supernatant was decanted into a test tube as leachate. Acid extraction was conducted at the Key Laboratory of Environmental Geochemistry of the Institute of Geochemistry, Chinese Academy of Sciences.

The major elements (Al, Fe, and Mn) in the digested soil samples and leachates were measured with an Inductively Coupled Plasma-Optical Emission Spectrometer (ICP-OES) in the Capital Circle Ecological Environment Laboratory at Capital Normal University. Trace elements were measured in solution with an Inductively Coupled Plasma-Mass Spectrometer (HR-ICP-MS) (Element I, Finnigan MAT Company) at the Beijing Research Institute of Uranium Geology. The analytical precision values for major and trace elements were less than 5% and 10%, respectively. REE concentrations were normalized to chondrite. Fractionation between LREEs and HREEs was quantified in accordance with $(La/Yb)_N$ ratio. Ce and Eu anomalies were calculated in accordance with the study of Taylor et al. (1986). In the present study, Ce and Eu anomalies were characterized by using δCe and δEu values, where δCe is defined as $(Ce)_N/[(La_N + Pr_N)/2] = Ce/Ce*$, and δEu is defined as $(Eu)_N/[(Sm_N + Gd_N)/2] = Eu/Eu*$.

Mass transfer coefficient (τ) was calculated to provide information about REE mobility during chemical weathering. The content of element (*j*) in the parent material (*p*) relative to that of immobile reference element (*i*) was used for standardization to assess mass changes in a gradually weathering material (*w*) (Anderson et al., 2002; Brimhall and Dietrich, 1987). τ was calculated using the following equation:

$$\tau_{i,j} = \{[(C_{j,w})/(C_{j,p})]/[(C_{i,w})/(C_{i,p})]\} - 1,$$

where $C_{j,w}$ and $C_{j,p}$ are the concentrations of element *j* in the soil sample and parent material, respectively, and $C_{i,w}$ and $C_{i,p}$ are the contents of the most immobile element (*i*) in the soil sample and parent material, respectively. A positive $\tau_{i,j}$ value indicates that element *j* is enriched in soils relative to that in a parent material, whereas a negative value indicates the depletion of element *j*. A $\tau_{i,j}$ value of zero indicates the immobility of element *j* in soil samples. In this study, we used the bedrock sample (HY and QZ-02) from each profile as the parent material for τ calculation. Zr, Ti, and Th are usually used as immobile elements. Although Th can be mobilized during intense tropical weathering (Du et al., 2012), Zr and Ti are more mobile during extreme weathering than Th (Braun et al., 1993; Ma et al., 2007b). Given the minor heterogeneity of parental Th-bearing minerals and limited migration and dissolution of these elements during weathering, minor Th mobilization will not significantly change the results when REE behavior in the profiles is considered (Berger et al., 2014;

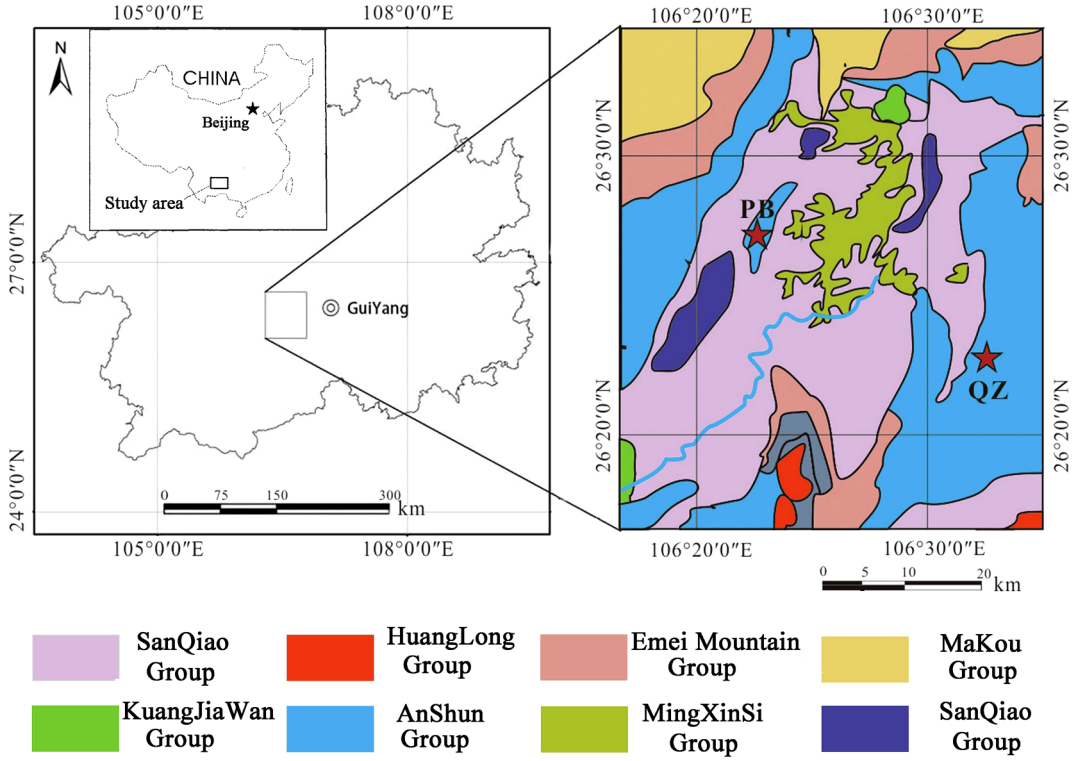

Fig. 1. Geological map of the Guizhou province and the two dolomite weathering profiles. The studied profiles are indicated on the map by stars (QZ = Qingzhen profile, PB = Pingba profile).

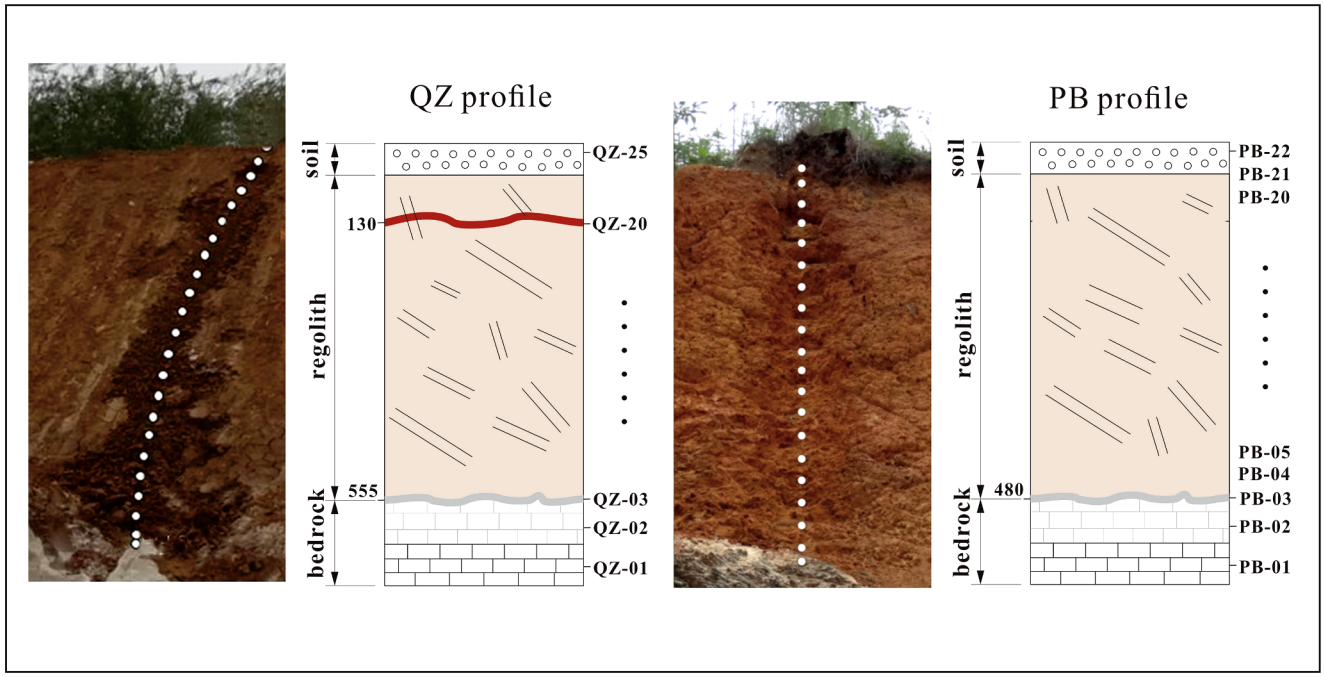

Fig. 2. Schematic representation of studied weathering profiles showing the sectional structure and sampling depth.

Janots et al., 2015). Th is more immobile and thus used as the reference element in this study.

3. Results

3.1. Major elements, pH, and TOC in soils and/or leachates.

Selected elemental data (including Th, Al, Fe, and Mn), pH, and TOC in the soil samples and leachates are listed in Tables 4 and 5. TOC contents are approximately 0.31% in most samples from QZ profile and increases at the surface layer, whereas its minimum value (0.19%) is obtained at the weathering front (QZ-07). The lower part of the profile has significantly higher pH (close to 7) than the upper part (less than 5). The TOC contents of the PB soil samples vary from 0.23% to 0.85% (except PB-22 = 2.09%). The pH gradually decreases with increasing depth as evidenced by the pH values from PB-3 (7.02) to PB-20 (4.67).

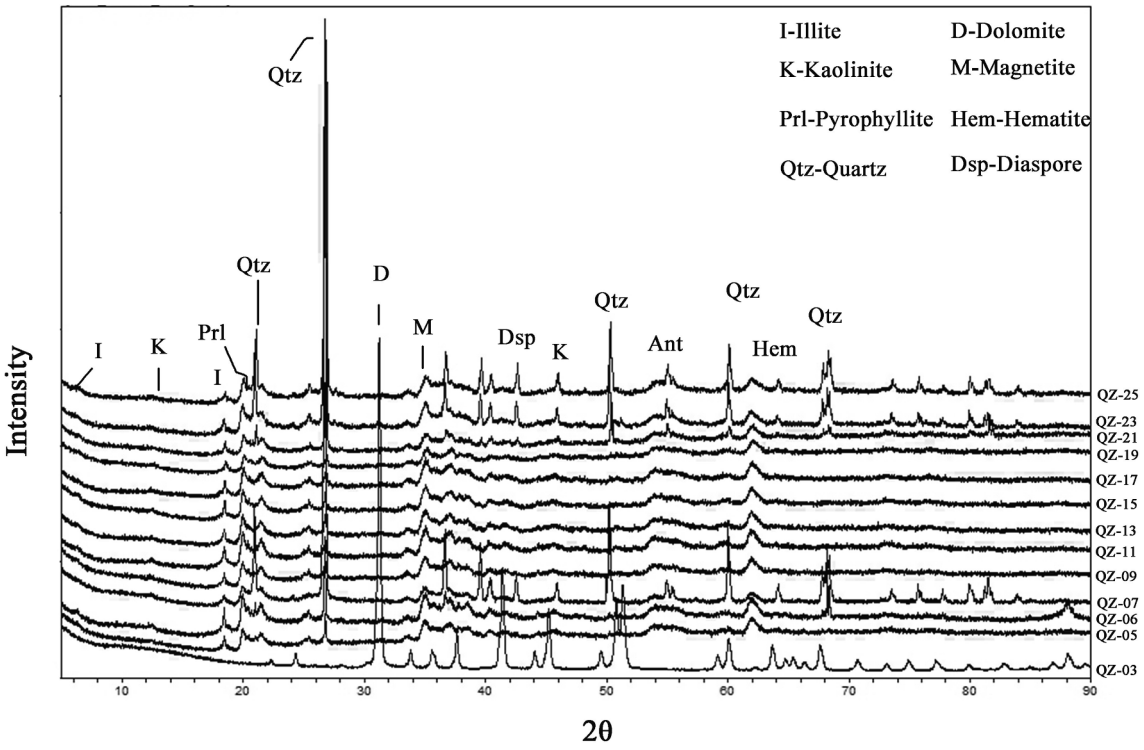

Fig. 3. X-ray diffraction graph showing mineral composition for Qingzhen profile.

Al content in the QZ soil samples is mostly 17%, with minimum and maximum values of 8.83% (QZ-07) and 17.85% (QZ-16), respectively. The concentration of Al in leachate is approximately 1.5%, with a minimum of 0.95% at QZ-07. The lowest Fe contents are obtained in the QZ-24 soil sample (5.35%) and leachate (1.36%). The highest Fe concentrations are obtained in the QZ-20 soil sample (21.33%) and leachate (5.42%). The highest Mn contents are 0.28% (QZ-19 soil sample) and 0.18% (QZ-19 leachate). Ferruginous crust appears near the soil layers of QZ-19 and QZ-20, which contain high concentrations of Fe and Mn. Al content in the PB soil samples fluctuates between 9.55% and 16.24% and shows an increasing trend with depth. In the leachates, the Al contents are approximately 2%. The concentrations of Fe in the PB profile are approximately 10% in the soil samples and 2% in the leachates. Mn is enriched in the lower parts of the soil samples and leachates in the PB profile.

3.2. REE characteristics of soil samples

REE contents and relevant parameters from the QZ profile are summarized in Table 1. The REE contents in the dolomite samples (QZ-01–QZ-03) in the QZ profile show remarkable negative Ce anomalies (Ce/Ce* = 0.29 in QZ-01, Ce/Ce* = 0.10 in QZ-02, and Ce/Ce* = 0.03 in QZ-03), moderate to weak Eu anomalies (Eu/Eu* = 0.73–0.93), and high $(La/Yb)_N$ values especially in QZ-03 (10.51). The patterns show remarkable negative Ce anomalies in rock powder (0.03) and rock–soil interface layer (0.21). Furthermore, the rock–soil interface sample (QZ-04) has the highest REE concentration (ΣREE = 1814.19 ppm) and lowest fractionation degree [$(La/Yb)_N$ = 3]. The proportion of LREEs (LREE%; 62.3%) and the ratio between LREEs and HREEs (1.65) are minimal in the profile. ΣREE values range from 167.4 ppm (QZ-20) to 1814.2 ppm (QZ-04), and LREEs and HREEs in the weathering profile vary considerably (ranging from 137.1 ppm to 1129.7 ppm and from 30.29 ppm to 684.49 ppm, respectively), whereas $(La/Yb)_N$ range from 3.00 to 8.92, exhibiting the high enrichment of LREEs relative to that of HREEs.

The samples in the lower part of the profile (QZ-05–QZ-07) have lower degree of LREE enrichment [$(La/Yb)_N$ = 2.70–4.30] and moderate Ce anomalies (0.62–0.81). Their REE patterns are similar to those of the parent rock samples (QZ-01 and QZ-02), showing the close inheritance from the bedrock in soil samples. The moderately negative Eu anomaly is observed in all samples. From the weathering front to the upper part of the profile, LREEs tend to become enriched, $(La/Yb)_N$ increases, and ΣLREE/ΣHREE becomes more remarkable (5.17–7.10) from samples QZ-13 to QZ-19. Meanwhile, positive Ce anomalies (δCe = 1.02–2.83) are noticeable in the upper part of the profile. The ferruginous crust (QZ-20) has the lowest ΣREE (167.39 ppm), which is similar to that of the upper continental crust (168.4 ppm) (Taylor and McLennan, 1985).

The chondrite-normalized REE pattern of the rock powder (PB-03) displays remarkable Ce anomaly (Ce/Ce* = 0.11), moderate Eu anomaly (Eu/Eu* = 0.69), and low $(La/Yb)_N$ (5.24). Sample PB-04 from the rock–soil interface has the highest REE value and displays the most negative Ce anomaly (Ce/Ce* = 0.09). The ΣREE values of the PB profile range from 255.8 ppm (PB-13) to 4091 ppm (PB-04), and the LREE and HREE values range from 198.44 ppm to 3091 ppm and from 52.83 ppm to 1000.2 ppm (Table 2), respectively. The ΣLREE/ΣHREE values are nearly consistent (approximately 4) except from PB-08 to PB-10. In the upper part of the profile, negative Ce anomaly decreases (Ce/Ce* = 0.56–0.99, except from PB-08 to PB-10), and moderate to weak positive Ce anomalies appear (Ce/Ce* = 1.04–1.43). From the lower to the upper parts of the profile, the $(La/Sm)_N$ and $(Gd/Yb)_N$ values tend to increase and decrease, respectively, indicating MREE enrichment in the lower part of the profile. Meanwhile, LREEs tend to become more enriched, that is, $(La/Yb)_N$ increases from 6.59 to 9.15. Three samples (PB-08–PB-10) near the weathering front show remarkable positive Ce anomalies (δCe = 1.79–3.78) and large ΣLREE/ΣHREE values (5.29–9.72).

$\tau_{Th,j}$ ($\tau_{Th,REE}$, $\tau_{Th,Al}$, $\tau_{Th,Fe}$, and $\tau_{Th,Mn}$) values were calculated for both profiles (Fig. 4). The $\tau_{Th,j}$ values for LREEs and HREEs are close to −1 in the regolith, indicating that REEs are fully depleted. The mass transfer coefficients of LREEs and HREEs are greater than zero in the rock powder layer and rock–soil interface, where REE contents increase drastically. This variation is mainly attributed to volumetric changes. Ji et al. (2004a, b) used a mass balance approach to quantify the mass fluxes of elements and found that large volume changes occur during dolomite weathering, namely, non-isovolumetric weathering, at the

Table 1
REE concentrations of samples from Qingzhen profile.

Sample	QZ-01	QZ-02	QZ-03	QZ-04	QZ-05	QZ-06	QZ-07	QZ-08	QZ-09	QZ-10	QZ-11	QZ-12
Depth (m)			5.55	5.3	5.05	4.80	4.55	4.30	4.05	3.80	3.55	3.30
La	2.71	3.01	58.60	243.00	152.00	112.00	62.10	102.00	91.10	71.10	65.80	63.40
Ce	1.53	0.76	4.14	138.00	274.00	205.00	90.80	340.00	211.00	137.00	194.00	188.00
Pr	0.60	1.03	22.20	108.00	48.90	33.20	20.30	28.00	21.70	14.70	14.10	12.90
Nd	2.98	4.51	97.60	467.00	204.00	136.00	85.50	112.00	84.30	56.00	53.60	48.30
Sm	0.44	1.28	23.40	142.00	49.20	30.50	21.70	24.60	17.70	10.90	10.30	9.25
Eu	0.14	0.31	4.60	31.70	10.40	6.48	4.48	5.10	3.75	2.21	2.03	1.82
Gd	0.47	1.09	15.90	122.00	40.30	25.90	16.80	21.00	15.70	9.85	9.45	8.58
Tb	0.10	0.17	2.67	24.90	7.87	5.11	3.53	4.25	3.26	2.03	1.86	1.68
Dy	0.47	1.07	10.70	121.00	38.30	25.80	18.20	22.30	17.00	11.00	10.10	9.19
Ho	0.09	0.14	1.56	20.30	6.50	4.49	3.15	3.93	3.07	2.06	1.91	1.74
Er	0.21	0.45	3.99	54.50	18.30	12.60	8.93	11.40	9.00	6.21	5.77	5.32
Tm	0.06	0.09	0.62	8.80	3.18	2.24	1.66	2.08	1.64	1.14	1.08	0.97
Yb	0.26	0.37	3.76	54.70	20.90	14.30	11.20	13.90	10.80	7.49	7.05	6.40
Lu	0.03	0.03	0.49	7.29	2.72	1.92	1.48	1.86	1.43	1.00	0.95	0.88
Y	2.83	2.28	15.70	271.00	97.90	72.10	40.50	61.50	53.40	41.80	38.30	35.10
ΣREE	12.94	16.58	265.93	1814.19	974.47	687.64	390.33	753.92	544.85	374.49	416.30	393.53
REE-Ce	11.41	15.82	261.79	1676.19	700.47	482.64	299.53	413.92	333.85	237.49	222.30	205.53
ΣLREE	8.40	10.89	210.54	1129.70	738.50	523.18	284.88	611.70	429.55	291.91	339.83	323.67
ΣHREE	4.53	5.69	55.39	684.49	235.97	164.46	105.45	142.22	115.30	82.58	76.47	69.86
ΣLREE/ΣHREE	1.85	1.91	3.80	1.65	3.13	3.18	2.70	4.30	3.73	3.54	4.44	4.63
LREE%	64.95	65.69	79.17	62.27	75.78	76.08	72.98	81.14	78.84	77.95	81.63	82.25
HREE%	35.05	34.31	20.83	37.73	24.22	23.92	27.02	18.86	21.16	22.05	18.37	17.75
δEu	0.93	0.79	0.73	0.74	0.71	0.70	0.72	0.69	0.69	0.65	0.63	0.62
δCe	0.29	0.10	0.03	0.21	0.76	0.81	0.62	1.53	1.14	1.02	1.53	1.58
$(La/Yb)_N$	7.11	5.46	10.51	3.00	4.90	5.28	3.74	4.95	5.69	6.40	6.29	6.68
$(La/Sm)_N$	3.84	1.48	1.58	1.08	1.94	2.31	1.80	2.61	3.24	4.10	4.02	4.31
$(Gd/Yb)_N$	1.46	2.36	3.41	1.80	1.56	1.46	1.21	1.22	1.17	1.06	1.08	1.08

Sample	QZ-13	QZ-14	QZ-15	QZ-16	QZ-17	QZ-18	QZ-19	QZ-20	QZ-21	QZ-22	QZ-23	QZ-24	QZ-25
Depth (m)	3.05	2.80	2.55	2.30	2.05	1.80	1.55	1.30	1.05	0.80	0.55	0.30	0.05
La	61.10	56.20	54.90	55.50	49.50	43.60	46.70	29.00	41.60	43.50	46.20	44.50	43.80
Ce	216.00	244.00	173.00	184.00	175.00	144.00	245.00	75.30	93.70	99.30	122.00	107.00	105.00
Pr	12.30	10.70	10.80	10.50	9.52	8.24	9.29	5.87	8.01	8.30	8.96	8.82	8.18
Nd	46.20	40.30	40.90	38.70	34.70	29.80	35.30	22.10	29.90	30.20	32.70	32.70	30.70
Sm	8.58	7.64	7.51	6.96	5.92	5.26	6.17	4.03	5.28	5.28	5.34	5.34	5.09
Eu	1.72	1.58	1.43	1.39	1.18	1.04	1.21	0.80	0.99	0.91	0.94	0.94	0.93
Gd	7.91	7.35	6.67	6.54	5.61	4.94	6.01	3.56	4.96	4.40	4.76	4.74	4.63
Tb	1.57	1.42	1.28	1.22	1.03	0.90	1.04	0.68	0.88	0.79	0.83	0.86	0.83
Dy	8.19	7.44	6.79	6.77	5.37	4.87	5.37	3.59	4.86	4.36	4.43	4.68	4.55
Ho	1.62	1.46	1.34	1.35	1.12	1.00	1.14	0.73	1.01	0.90	0.90	0.98	0.93
Er	4.95	4.29	4.03	4.15	3.43	3.06	3.56	2.25	3.15	2.83	2.85	2.93	3.01
Tm	0.89	0.81	0.78	0.75	0.62	0.55	0.63	0.42	0.57	0.52	0.53	0.52	0.54
Yb	5.96	5.39	5.07	5.08	4.21	3.85	4.23	2.85	3.82	3.49	3.49	3.60	3.67
Lu	0.82	0.74	0.70	0.70	0.59	0.55	0.61	0.41	0.55	0.50	0.49	0.51	0.51
Y	33.40	28.90	28.00	30.90	25.00	23.20	25.80	15.80	23.40	22.60	28.60	24.50	24.80
ΣREE	411.21	418.22	343.20	354.52	322.81	274.86	392.06	167.39	222.67	227.88	263.02	242.62	237.16
REE-Ce	195.21	174.22	170.20	170.52	147.81	130.86	147.06	92.09	128.97	128.58	141.02	135.62	132.16
ΣLREE	345.90	360.42	288.54	297.05	275.82	231.94	343.67	137.10	179.48	187.49	216.14	199.30	193.70
ΣHREE	65.31	57.80	54.66	57.47	46.99	42.92	48.39	30.29	43.19	40.40	46.88	43.32	43.46
ΣLREE/ΣHREE	5.30	6.24	5.28	5.17	5.87	5.40	7.10	4.53	4.16	4.64	4.61	4.60	4.46
LREE%	84.12	86.18	84.07	83.79	85.44	84.38	87.66	81.90	80.60	82.27	82.18	82.15	81.68

(*continued on next page*)

Table 1 (*continued*)

Sample	QZ-13	QZ-14	QZ-15	QZ-16	QZ-17	QZ-18	QZ-19	QZ-20	QZ-21	QZ-22	QZ-23	QZ-24	QZ-25
Depth (m)	3.05	2.80	2.55	2.30	2.05	1.80	1.55	1.30	1.05	0.80	0.55	0.30	0.05
HREE%	15.88	13.82	15.93	16.21	14.56	15.62	12.34	18.10	19.40	17.73	17.82	17.85	18.32
δEu	0.64	0.64	0.62	0.63	0.63	0.62	0.61	0.64	0.59	0.57	0.57	0.57	0.59
δCe	1.90	2.39	1.71	1.83	1.94	1.83	2.83	1.39	1.24	1.26	1.44	1.30	1.34
$(La/Yb)_N$	6.91	7.03	7.30	7.37	7.93	7.64	7.44	6.86	7.34	8.40	8.92	8.33	8.05
$(La/Sm)_N$	4.48	4.63	4.60	5.02	5.26	5.21	4.76	4.53	4.96	5.18	5.44	5.24	5.41
$(Gd/Yb)_N$	1.07	1.10	1.06	1.04	1.08	1.04	1.15	1.01	1.05	1.02	1.10	1.06	1.02

All concentrations are normalized to the bulk sample and given in ppm.
The Ce anomaly($\delta Ce = Ce_N/[(La_N + Pr_N)/2]$)and Eu anomaly($\delta Eu = Eu_N/[(Sm_N + Gd_N)/2]$)were calculated.
Listed also the $(La/Yb)_N = ((La/La_N)/(Yb/Yb_N))$, $(La/Sm)_N = ((La/La_N)/(Sm/Sm_N))$ and $(Gd/Yb)_N = ((Gd/Gd_N)/(Yb/Yb_N))$ ratios indicating the degree of REE.

bedrock to the regolith horizon. During dolomite weathering, more than 90% of the volume changes, and insoluble residues account for only 1% of the dolomite total mass. The large volumetric change causes the enrichment of elements, resulting in $\tau_{Th,j}$ values greater than 0.

3.3. REE characteristics of leachates

Chemical leaching aims to understand the distribution, migration, and geochemical behavior of REEs during supergene weathering (Sholkovitz, 1989). The leaching results of the soil samples from the QZ profile are listed in Table 3. The leachate ratio of each element in the leachate was determined by the formula: leachate ratio (%) = (element content in the 1 mol/L HCl leachate/element content in the whole rock) × 100 (Ma et al., 2007b). The ΣREE values range from 57.82 ppm (QZ-20) to 1360.39 ppm (QZ-04), and the leachate ratio decreases from the bottom (QZ-04 = 88.67%) to the upper layers (QZ-24 = 16.67%) of the profile. Simultaneously, ΣLREE/ΣHREE values increase from 1.56 (QZ-04) to 11.64 (QZ-24), indicating that LREEs are more easily removed than HREEs during the leaching process. This result is confirmed by LREE enrichment (except for Ce and Eu anomalies) in the leachate chondrite-normalized REE pattern (Fig. 6). The REE pattern of sample QZ-25 has a chondrite-normalized La_N value of 28.17, thus decreasing the Yb_N value to 1.13, with the largest $(La/Yb)_N$ (25.02) in the QZ profile. Compared with soil samples, leachates have large $(La/Yb)_N$ (2.36–25.02) and $(Gd/Yb)_N$ (1.40–3.64) and small $(La/Sm)_N$ (0.77–5.2), indicating that LREEs are more likely to be leached than HREEs. The leachate shows remarkable negative Ce anomalies (0.14–0.99) in the lower part of the profile and positive Ce anomalies (1.12–2.86) in the upper part of the profile and moderate to weak Eu anomalies (0.62–0.83).

The leaching results of the PB profile are similar to those of the QZ profile. From the bottom to the top of the profile, ΣLREE/ΣHREE values increase from 2.35 (PB-04) to 9.14 (PB-17). By contrast, REE contents decrease from 2236.61 ppm (PB-04) to 68.02 ppm (PB-21) along with the leachate ratio ranging from 19.57% (PB-21) to 66.90% (PB-04). The ranges of $(La/Yb)_N$, $(Gd/Yb)_N$, and $(La/Sm)_N$ values are 5.28–15.64, 1.53–4.33, and 2.07–3.58, respectively. The leachates from the PB profile have scattering REE patterns characterized by weak Eu anomalies (0.68–0.85) compared with the whole rock samples (0.58–0.68).

The contents of Ce and REEs (except Ce) in the leachates and bulk samples and the variation of leachate ratio with profile depth are depicted in Fig. 7 (QZ profile) and 8 (PB profile). Ce shows inconsistent changes with other REEs. As shown in Fig. 7, the leachate ratio of Ce in the QZ profile is concentrated at approximately 39%, whereas that of REE–Ce gradually decreases from the lower (QZ-04 = 88.67%) to the upper (QZ-24 = 16.67%) parts of the profile. Results show that leachate ratio is inversely proportional to the residual time of the soil layer. From the soil surface to a depth of 3 m, leachate ratio in Ce is larger than the leachate ratios in other REEs. From the section below 3 m to the bedrock, the leachate ratio in Ce is smaller than that the leachate ratio in the other REEs. In Fig. 8, the leachate ratio of REE–Ce in the PB profile is lower than that in the QZ profile. A similar trend in leachate ratio, that is, the decrease from the lower (66.90%) to the upper (19.57%) parts of the profile, is observed. The leachate ratio of Ce in the PB profile is higher than that in the QZ profile, which clusters at approximately 42%, and is lower than that of REE-Ce in the section from 3 m below the surface to the bedrock. Leachate ratio is indirectly related to the elemental contents in the sample.

4. Discussion

4.1. REE mobilization and fractionation during chemical weathering

REEs are known to be present as coatings or impurities dispersed in multiple minerals, oxides, and supergene minerals, such as

rhabdophane, florencite, and cerianite, and adsorbed on clay minerals. (Jin et al., 2017; Palumbo et al., 2001). During weathering and pedogenesis, REE-bearing minerals are dissolved, and REEs are released into the soil and transferred by soil solution. REE solubility is low, whereas the dissolved portion has good affinity to minerals (clay and Fe-oxides) via mechanisms, such as co-precipitation, adsorption, and surface complex formation (Cao et al., 2001; Galán et al., 2007; Ma et al., 2011; Yusoff et al., 2013). According to XRD analysis (Fig. 3), quartz content in the upper part of the soil increases, whereas REE-containing authigenic minerals and clay minerals decrease as weathering proceeds, resulting in REE depletion in the upper weathering profiles compared with the lower parts (Braun et al., 1998; Nesbitt and Markovics, 1997). This phenomenon is an important reason for REE enrichment in the lower parts of the profiles and is consistent with the reports of previous studies that REE content decreases with increasing weathering degree (Öhlander et al., 1996; Taunton et al., 2000). Some studies demonstrated that Fe, Al, P, and Mn compounds does not contribute much to REE enrichment in the basalt profile and terra rossa (Ma et al., 2007b; Feng, 2010). In the present study, REE content has no good correlation with Al, Fe, and Mn contents, but they show consistent changes in some layers. As shown in Fig. 4, Al, Fe, and Mn are enriched with REE enrichment near the weathering front of the QZ profile (dash area), whereas they are depleted along with REEs in the lower samples of PB (dash area). pH and organic matter may control REE mobility. REE adsorption usually increases with pH (Aja, 1998; Coppin et al., 2002), and organic matter enhances REE mobility by complexing with organic colloids. These phenomena lead to the significant depletion of REEs in the acid upper part of profile and relative enrichment in the lower samples. When REEs are transported downward to the lower part of the QZ profile, organic matter largely decomposes, resulting in relative enrichment of REEs in this depth (dash area in Fig. 4). Therefore, we think that REE enrichment in the lower part of profile may be related to TOC. A particularly high TOC concentration is noted in sample QZ-03 possibly due to the volumetric change in initial carbonate weathering. Weathering leads to a 90% decrease in bedrock volume, whereas organic matter accumulates in the rock powder layer. TOC content decomposes as weathering proceeds.

Except for some soluble phosphate minerals, 1 N HCl does not dissolve minerals in the regolith. REEs in leachates mainly comprise an adsorbed clay, adsorbed amorphous Mn–Fe (hydro)oxides, and dissolved phosphate minerals (Song and Choi, 2009). The leachate ratio of the two profiles increase from the top to the bottom with increasing REE content. The largest leaching rate occurs in the REE enrichment layer of the PB profile (dash area in Fig. 4), confirming that REEs are transported from the upper part to the lower part, and sorption likely plays an important role in REE transfer.

The fractionation between LREEs and HREEs is usually quantified by $(La/Yb)_N$ ratios or ΣLREE/ΣHREE values (Laveuf and Cornu, 2009). The three main reasons put forward to explain the fractionation of REEs in weathering profiles are as follows: (1) oxidation–reduction environment, pH, and other weathering conditions (Braun et al., 1990; Braun et al., 1998); (2) leaching of primary REE-bearing minerals; and (3) influences of secondary minerals, such as Mn–Fe (hydro)oxides, clay minerals, and phosphates, which are bound to REEs or precipitated with REEs (Braun et al., 2018; Kuss et al., 2001; Yang et al., 2002). $(La/Yb)_N$ values show pronounced REE fractionation in the QZ and PB profiles during weathering. LREEs are more enriched than HREEs. Increasing ΣLREE/ΣHREE in the topsoil results in increased $(La/Yb)_N$ values in both profiles. This condition was reported by Banfield and Eggleton (1989) in the study of granodiorite massif in Australia. The different distributions between the lower and upper parts of profiles are interpreted as follows: HREEs denote stable compounds in the solution that is relatively preferentially transported downward, whereas LREEs are easily absorbed on clay minerals (da Silva et al., 2017; Duddy, 1980).

In both profiles (QZ and PB), the chondrite-normalized REE distribution patterns of soil samples (Fig. 5) and leachates (Fig. 6) have the same trend, but their values are different. The $(La/Yb)_N$ and $(Gd/Yb)_N$ values in the leachates are systematically higher than those in the soil samples (Tables 1–3). The $(La/Yb)_N$ values indicate an increase in REE fractionation degree. Thus, the probability for this increase to occur increases as weathering continues. HREEs and part of LREEs usually migrate through weathering profiles via soil solution, and residual LREEs may be incorporated into secondary minerals, such as clay minerals, carbonates, and Fe- and Mn-oxides, which may be dissolved with further weathering. The overall trends of soils from the QZ and PB profiles exhibit REE fractionation during LREE enrichment and HREE depletion.

LREE/HREE ratio has been widely regarded as a proxy to REE fractionation and provenance tracing in many geological processes (Dou et al., 2010; Jung et al., 2012; Riebe et al., 2017). Th has a relatively stable geochemical behavior during geological processes compared with REEs. Therefore, it is typically used as reference element in element migration studies. The variation in REE contents can be measured by ΣREE/Th ratios of soil samples during weathering.

Fig. 9 exhibits the relationship of LREE/HREE and ΣREE/Th ratios of QZ and PB soil samples, respectively. The ratios of LREE/HREE have narrow variation ranges relative to those of ΣREE/Th, and the ratios are not correlated with those of ΣREE/Th in PB and QZ soil profiles. PB-09 and PB-10 samples have high LREE/HREE ratios, which can be interpreted by water–rock interaction around the weathering front. A distinct variation trend is displayed between LREE/HREE and ΣREE/Th ratios in the PB and QZ leachates (Fig. 9). In the PB leachate, a general exponential decline trend has marked the increase in LREE/HREE ratios (up to 9.14 in PB-17) along with decreasing ΣREE/Th. A similar trend is observed in the QZ leachate. The LREE/HREE ratios in the QZ leachate gradually increase from 1.56 (QZ-04) to 11.64 (QZ-24) as ΣREE/Th decreases from the lower (QZ-05 = 38.68) to the upper (QZ-20 = 4) regolith parts, suggesting that HREEs have higher mobility than LREEs due to the ability of HREEs to easily form bicarbonate and organic complexes in a solution; by contrast, LREEs tend to be adsorbed on secondary minerals (e.g., clay minerals) (Laveuf and Cornu, 2009). Therefore, LREE enrichment and HREE depletion occurs in leachates. From the bedrock (includes rock powder and rock–soil interface) to the lower regolith (below 4 m in QZ profile and 3.8 m in PB profile), which is a known chemical weathering process, ΣREE/Th decreases sharply, whereas the variation in LREE/HREE varies slightly. From the lower to the upper regolith parts (above 4 m in the QZ profile and 3.8 m in the PB profile), LREE/HREE increases, whereas ΣREE/Th changes slightly. This LREE enrichment signal indicates that pedogenesis results in greater REE fractionation (Ni et al., 2017). This observation indicates an important weathering and pedogenetic trend with REE depletion and fractionation from exchangeable components in an acid leaching environment.

4.2. Ce anomalies in leachates and whole rock samples

Many studies demonstrated that Ce is sensitive to changes in redox environments, clay minerals, Fe–Mn (hydro)oxides, and organic materials (Feng, 2010; Laveuf et al., 2012; Vázquez-Ortega et al., 2015). Ce has more than one oxidation states that induce Ce anomalies due to redox reactions, which record the changes in redox conditions during pedogenetic processes. Ce (III) is soluble in a reduced environment and is converted into the insoluble Ce (IV) oxidation state in an oxidized environment. This mechanism may induce the variation in δCe values and Ce fractionation during weathering processes especially in surface environments. The behavior of Ce is different from that of other REEs in this study. Strong Ce anomalies occur in the QZ profile as shown by the remarkable negative and positive Ce anomalies in the lower and upper parts of the profile, respectively (Table 1). Almost all carbonate rocks display a negative Ce anomaly due to coordination numbers and ionic radii (Kanazawa and Kamitani, 2006; Laveuf and Cornu, 2009). Thus, we could infer that the negative Ce anomaly near the base profile (dash area in Fig. 10) is inherited from the dolomite bedrock. The maximization of negative Ce anomaly is evident in the QZ rock–soil interface QZ-04

Table 2
REE concentrations of samples from Pingba profile.

Sample	HY	PB-03	PB-04	PB-05	PB-06	PB-07	PB-08	PB-09	PB-10	PB-11	PB-12	PB-13	PB-14	PB-15	PB-16	PB-17	PB-18	PB-19	PB-20	PB-21	PB-22
Depth (m)	7.254.80		4.55	4.30	4.05	3.80	3.55	3.30	3.05	2.80	2.55	2.30	2.05	1.80	1.55	1.30	1.05	0.80	0.55	0.30	0.05
La	2.78	35.60	922.00	178.00	170.00	167.00	87.40	76.70	64.40	56.40	53.80	52.00	49.30	48.70	52.70	51.60	54.50	53.10	48.80	54.20	57.00
Ce	1.91	9.37	201.00	232.00	224.00	200.00	310.00	397.00	451.00	100.00	93.10	90.30	101.00	124.00	137.00	137.00	124.00	112.00	107.00	104.00	101.00
Pr	0.73	11.00	301.00	47.80	47.00	44.90	19.90	16.70	12.80	10.50	10.50	9.63	10.10	10.20	10.80	10.30	11.00	10.30	9.45	10.60	11.20
Nd	4.09	49.80	1298.00	200.00	191.00	184.00	77.10	65.70	47.70	40.10	41.50	38.10	39.40	39.80	42.20	40.90	43.40	39.80	36.60	38.50	40.50
Sm	1.61	13.00	306.00	45.00	41.40	39.30	16.50	12.40	8.41	7.14	8.04	7.02	7.49	7.30	7.73	7.07	7.65	7.11	6.26	6.56	6.92
Eu	0.62	3.18	62.80	9.07	8.49	7.74	3.26	2.54	1.74	1.46	1.62	1.39	1.45	1.42	1.43	1.33	1.45	1.36	1.20	1.20	1.24
Gd	2.75	15.20	247.00	36.60	34.70	31.70	15.70	12.10	8.69	6.99	8.10	6.96	7.25	7.03	7.33	6.86	7.28	6.71	5.80	6.14	6.36
Tb	0.43	2.85	48.20	7.19	6.53	5.97	2.96	2.16	1.36	1.26	1.52	1.26	1.25	1.29	1.30	1.20	1.27	1.22	1.07	1.17	1.12
Dy	1.58	12.90	209.00	34.50	30.50	27.50	14.80	10.50	7.09	6.42	8.38	6.72	6.80	6.52	6.53	6.50	6.55	6.35	5.68	6.22	6.10
Ho	0.21	2.04	32.00	5.69	5.17	4.47	2.75	1.92	1.35	1.31	1.63	1.37	1.34	1.34	1.33	1.30	1.37	1.22	1.18	1.24	1.22
Er	0.43	5.01	84.40	15.30	14.40	12.50	7.71	5.56	4.16	3.92	4.89	4.17	4.03	3.92	4.15	4.07	4.14	3.78	3.68	3.71	3.60
Tm	0.07	0.76	14.80	2.59	2.46	2.19	1.34	0.99	0.72	0.66	0.85	0.72	0.69	0.67	0.69	0.66	0.73	0.66	0.62	0.64	0.62
Yb	0.39	4.58	98.10	18.20	16.50	14.30	9.13	6.64	4.79	4.31	5.35	4.63	4.60	4.45	4.60	4.38	4.59	4.48	4.04	4.26	4.20
Lu	0.06	0.57	12.70	2.40	2.20	1.90	1.24	0.87	0.65	0.58	0.72	0.64	0.63	0.63	0.65	0.63	0.61	0.64	0.56	0.58	0.55
Y	3.06	19.00	254.00	70.80	66.80	64.10	41.50	39.20	31.50	29.50	31.30	30.90	30.20	28.80	29.90	32.10	34.30	32.80	30.20	33.20	32.40
ΣREE	17.66	184.85	4091.00	905.14	861.15	807.57	611.29	650.98	646.36	270.55	271.29	255.80	265.53	286.07	308.34	305.89	302.84	281.53	262.14	272.22	274.03
REE-Ce	15.75	175.48	3890.00	673.14	637.15	607.57	301.29	253.98	195.36	170.55	178.19	165.50	164.53	162.07	171.34	168.89	178.84	169.53	155.14	168.22	173.03
ΣLREE	11.74	121.95	3090.80	711.87	681.89	642.94	514.16	571.04	586.05	215.60	208.56	198.44	208.74	231.42	251.86	248.20	242.00	223.67	209.31	215.06	217.86
ΣHREE	5.92	62.90	1000.20	193.27	179.26	164.63	97.13	79.94	60.31	54.95	62.73	57.36	56.79	54.65	56.48	57.69	60.84	57.86	52.83	57.16	56.17
ΣLREE/ ΣHREE	1.98	1.94	3.09	3.68	3.80	3.91	5.29	7.14	9.72	3.92	3.32	3.46	3.68	4.23	4.46	4.30	3.98	3.87	3.96	3.76	3.88
LREE%	66.48	65.97	75.55	78.65	79.18	79.61	84.11	87.72	90.67	79.69	76.88	77.58	78.61	80.90	81.68	81.14	79.91	79.45	79.85	79.00	79.50
HREE%	33.52	34.03	24.45	21.35	20.82	20.39	15.89	12.28	9.33	20.31	23.12	22.42	21.39	19.10	18.32	18.86	20.09	20.55	20.15	21.00	20.50
δEu	0.90	0.69	0.70	0.68	0.68	0.67	0.62	0.63	0.62	0.63	0.61	0.61	0.60	0.61	0.58	0.58	0.59	0.60	0.61	0.58	0.57
δCe	0.31	0.11	0.09	0.61	0.60	0.56	1.79	2.67	3.78	0.99	0.94	0.97	1.09	1.34	1.38	1.43	1.22	1.15	1.20	1.04	0.96
$(La/Yb)_N$	4.85	5.24	6.34	6.59	6.95	7.87	6.45	7.79	9.06	8.82	6.78	7.57	7.23	7.38	7.72	7.94	8.01	7.99	8.14	8.58	9.15
$(La/Sm)_N$	1.09	1.72	1.90	2.49	2.58	2.67	3.33	3.89	4.82	4.97	4.21	4.66	4.14	4.20	4.29	4.59	4.48	4.70	4.90	5.20	5.18
$(Gd/Yb)_N$	5.74	2.68	2.03	1.62	1.70	1.79	1.39	1.47	1.46	1.31	1.22	1.21	1.27	1.27	1.29	1.26	1.28	1.21	1.16	1.16	1.22

We use the mixed bedrock HY from (Ji et al., 2004b) as the bedrock of PB profile.
All concentrations are normalized to the bulk sample and given in ppm.
The Ce anomaly($\delta Ce = Ce_N/[(La_N + Pr_N)/2]$)and Eu anomaly($\delta Eu = Eu_N/[(Sm_N + Gd_N)/2]$)were calculated.
Listed also the $(La/Yb)_N = ((La/La_N)/(Yb/Yb_N))$, $(La/Sm)_N = ((La/La_N)/(Sm/Sm_N))$ and $(Gd/Yb)_N = ((Gd/Gd_N)/(Yb/Yb_N))$ ratios indicating the degree of REE.

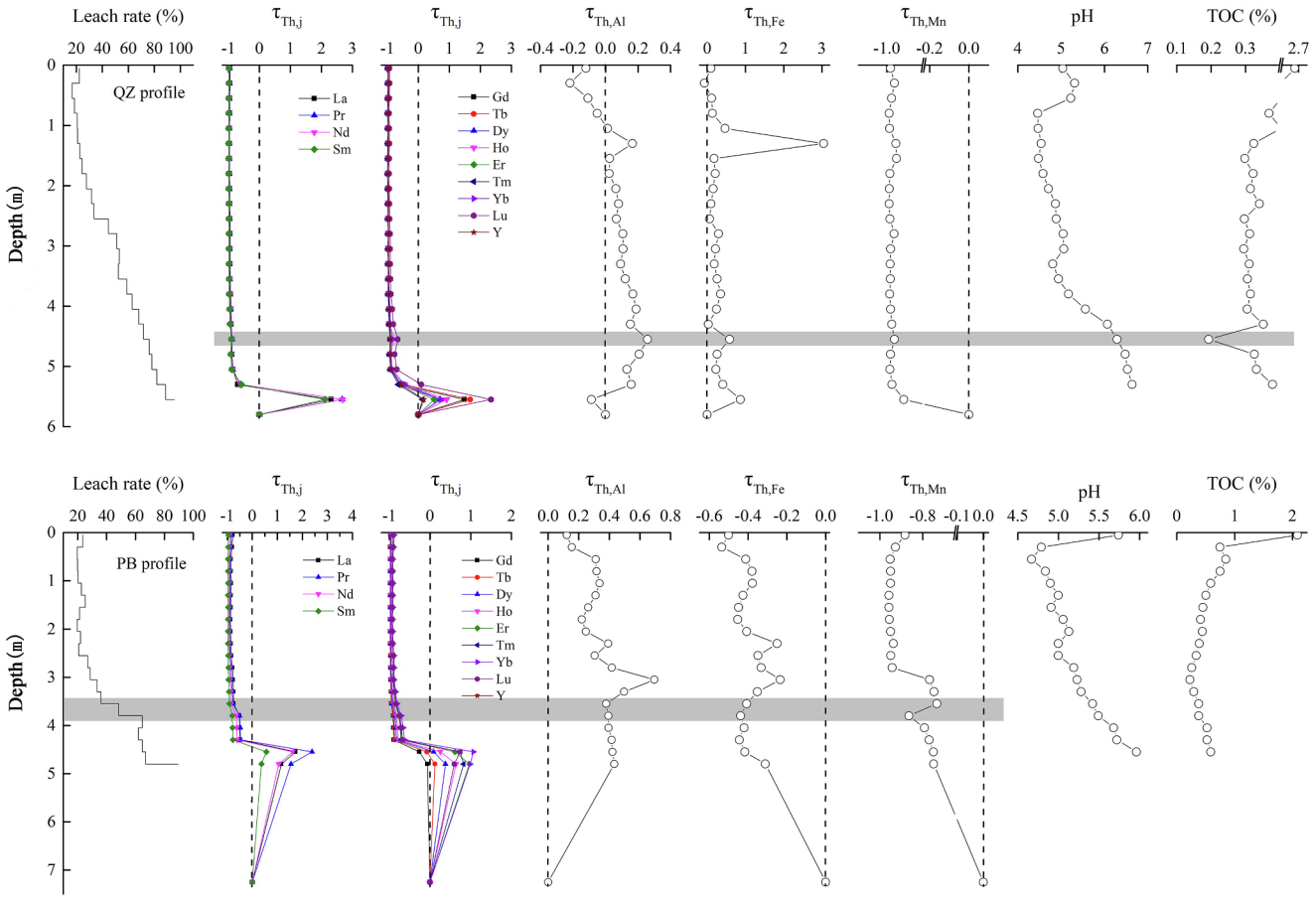

Fig. 4. Depth variations of leach rate, $\tau_{Th,REE}$, $\tau_{Th,Al}$, $\tau_{Th,Fe}$, $\tau_{Th,Mn}$, pH and TOC contents in Qingzhen and Pingba profiles.

(δCe = 0.21) and in the PB rock–soil interface PB-04 (δCe = 0.09). Meanwhile, REE content in the rock–soil interface from the QZ profile is 6.8 times of that of rock powder and 20 times of that in PB profile (Tables 1 and 2). The maximum negative Ce anomaly and REE enrichment may be due to the volume changes mentioned earlier. The large volume changes during weathering lead to the accumulation of REE-containing residues, resulting in an increase in REE content and absence of Ce. Previous studies in this area found that a small amount of apatite and rhabdophane–La exist in the lower part of the profile. These phosphate minerals contain REEs and have an obvious negative Ce anomaly (Feng et al., 2009; Ji et al., 2004b; Sun et al., 2002). Therefore, we believe that the presence of phosphate may be another important factor for rare earth enrichment and Ce anomaly at this layer (Banfield and Eggleton, 1989; Patino et al., 2003). Obvious differences in Ce behavior and highly variable Ce anomaly are observed in the PB profile. The Ce-anomaly in the lower part of the PB profile not only had negative anomalies but also demonstrated strong positive anomalies in specific samples, PB-08 (δCe = 1.79), PB-09 (δCe = 2.67), and PB-10 (δCe = 3.78). Notably, three samples are located close to the layer of weathering front, which occurs in water–rock interaction. Given the water–rock interaction, high ΣLREE/ΣHREE values and positive Ce anomalies are observed at the weathering front of the PB profile. A significantly positive Ce anomaly (δCe = 2.83) exists in sample QZ-19, which is near the ferruginous crust. Figs. 4 and 10 show that the ferruginous crust has a particularly positive Ce anomaly and is accompanied by high τFe and τMn contents, and Mn-oxides and Fe-oxyhydroxide indirectly affect the state of Ce. In the nodules from the deep-sea oceanic water, several studies show Ce scavenging at the surface of Mn- and Fe-oxide and hydroxide (Bau, 1999; Braun et al., 2018; Nakada et al., 2013). De Baar et al. (1988) studied the electrical potential change at the d-MnO_2 surface and proposed that Ce (III) is oxidized by d-MnO_2. They found that in solution without dissolved O_2, Ce oxidation is due to proton transfer between Ce (III) and d-MnO_2. Because the different experimental setting Ohta and Kawabe (2001) did not get the consistent result with De Carlo et al. (1998) that Mn(IV) reduced to Mn (II) due to Ce (III) oxidation reaction at the d-MnO_2 surface, but they also suggested that Ce (III) is oxidized to Ce (IV) by d-MnO_2. Ohta and Kawabe (2001) proposed that dissolved Ce (III) can be oxidized by Fe oxyhydroxide under atmospheric conditions, as indicated by the results of the present study. Although no significant correlation is obtained among Ce anomaly, Fe, and Mn in the study profiles, a large Ce anomaly corresponds to high $\tau_{Th,Mn}$ and $\tau_{Th,Fe}$ values. This result indicates that Fe and Mn affect Ce anomaly. Meanwhile, oxygen is consumed during TOC decomposition in the middle profile, resulting in an anaerobic condition in the base profile. This phenomenon has been observed in both profiles (orange band in Fig. 10), along with high δCe and low TOC values.

Acid leaching experiments can provide useful information on REE behavior without the factors affecting redox conditions, such as Fe- and Mn-oxides and hydroxides, TOC, and pH. However, in hydrochloric leaching experiments, the migration of Ce is found to be different from that of other REEs (Figs. 7 and 8), demonstrating that Ce has distinctive migration and transformation behavior with other REEs. Thus, our finding provides new recognition on the indication of Ce anomaly for redox change. Therefore, Ce behavior must be considered when using Ce anomaly in studying the redox conditions of the weathered sedimentary soil.

4.3. Comparison of Y and Ho behavior during weathering and leaching processes

A pseudo-lanthanide containing an ionic radius and Ho are considered the same and have consequently similar geochemical

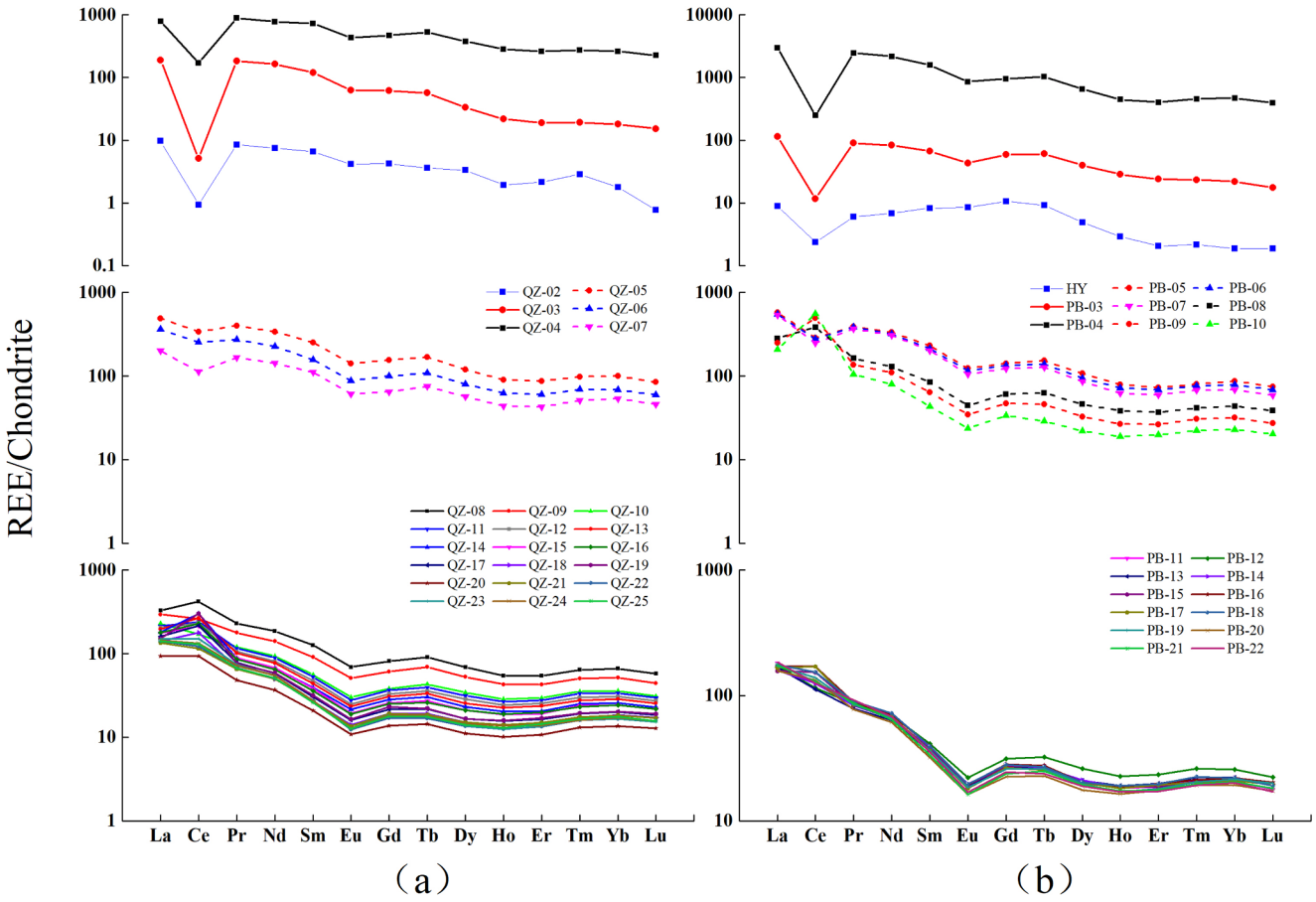

Fig. 5. Chondrite-normalized REE patterns of soil samples from Qingzhen profile (a) and Pingba profile (b). We use the mixed bedrock HY from (Ji et al., 2004b) as the bedrock of PB profile.

characteristics because its outer electron shell structure is similar to that of Y (Bau and Dulski, 1995; Thompson et al., 2013), whereas fractionation may exist between Y and Ho during weathering. The extent of fractionation is typically measured by Y/Ho ratio (Censi et al., 2007; Feng, 2010; Nozaki et al., 2000; Thompson et al., 2013). Y and Ho in the QZ samples show a significantly positive correlation (R^2 = 0.97, Fig. 11a), and the relationship of Y and Ho in leachates show a better positive correlation (R^2 = 0.98). Relative coherence is observed in the PB profile at R^2 of 0.97 (soils) and R^2 of 0.99 (leachates; Fig. 11b). This result suggests that the geochemical behavior of Y is more similar to that of Ho than that of the other REEs in HCl leachates and simulate the natural acid leaching process during soil formation. Many scholars demonstrated that the fractionation between Y and Ho occurs within oceans (Nozaki et al., 1997), rivers, and estuaries (Bau and Dulski, 1995; Bau et al., 1997) or during chemical weathering (Feng, 2010; Leybourne and Johannesson, 2008; Thompson et al., 2013). The good correlation between Y and Ho in soil samples and leachates demonstrates that the fractionation of Y and Ho occurs in the incipient processes of chemical weathering, such as dissolution of primary minerals especially Y-bearing minerals. The acid leaching experiment can lead to Y and/or Ho to desorb from oxides to solutions, and fractionation is not likely due to Y adsorption and/or Ho on Fe–Mn oxides. In soil samples of QZ and PB profiles, Y/Ho increases from the bottom to the top (ranging from 10.06 to 31.92 in QZ and ranging from 7.94 to 26.88 in PB). Leachates have a similar trend, but their values are lower than those of the soil samples (Fig. 12). The similar tendency of Y/Ho ratios in two profiles displays the strong inheritance of soil samples and leachates, suggesting the presence of slight fractionation between Y and Ho in the subsequent weathering process. The two profiles show an obvious negative correlation between pH and Y/Ho ratios (Fig. 13). As shown in Fig. 4, pH decreases from the bottom to the upper profiles contrary to the Y/Ho trend. In high pH ranges, the complexation of Ho with HCO_3^- or organic material is stronger than Y. Hence, Y shows a stronger tendency to co-precipitate with Fe oxyhydroxide related to other REEs, decreasing Y/Ho ratios (Leybourne and Johannesson, 2008). The acidic environment in the upper part of profiles hinders the complexation of Ho and HCO_3^-, making Ho easier to migrate (Quinn et al., 2006). The dissolution of Y-bearing phases, such as Fe-oxides, increases at lower pH (Thompson et al., 2013), which possibly results in increased Y/Ho ratios toward the upper profiles. Ho is lost easier than Y because of the leaching process, and thus Y/Ho ratios decrease with depth.

4.4. Cause of the red clay formation

The QZ profile shows in situ weathering characteristics by a clear and intact bedrock–rock soil interface–ferruginous crust–humus layer. Given the similar REE behavior characteristics of PB and QZ profiles, the PB profile is identified as an in situ weathering profile. REE distribution in the two profiles shows a pattern of certain regularity, which proves that the profiles have no evident addition from other external sources. In Fig. 14, the bedrocks of the two dolomite profiles and their overlying red soils display significantly positive correlation between Y and Yb contents. The correlation coefficients of the QZ and PB profiles are 0.98 and 0.97, respectively, confirming that the profiles are derived from their underlying bedrocks without the interference of other material sources. These results can be used to determine the provenance of carbonate rock weathering crust in karst regions. Wang et al. (1999) compared the mineral composition of acid-insoluble matter with overlying soils in a karst area and found that the two parts have similar mineral compositions.

Table 3
REE concentrations of the HCl leachates for both profile Qingzhen and Pingba.

Sample	QZ-03	QZ-04	QZ-06	QZ-08	QZ-10	QZ-12	QZ-14	QZ-16	QZ-18	QZ-20	QZ-22	QZ-24	QZ-25	PB-03	PB-04	PB-06	PB-08	PB-10	PB-12	PB-14	PB-16	PB-18	PB-20	PB-22
La	56.46	161.21	74.29	62.40	38.01	30.83	24.89	21.81	14.97	8.94	10.33	8.73	9.23	33.09	497.82	86.80	40.88	22.22	15.40	11.05	11.03	12.48	9.16	11.81
Ce	4.18	68.142	65.68	114.47	60.76	70.60	96.64	59.94	51.74	33.91	39.85	43.95	52.56	7.38	82.08	79.21	101.97	88.44	45.59	46.82	66.50	65.27	52.77	34.93
Pr	21.64	82.93	26.15	20.82	10.00	7.47	5.92	4.38	2.90	1.85	2.12	1.96	2.12	10.49	150.17	28.61	10.90	4.67	3.37	2.35	2.64	2.90	2.16	2.72
Nd	85.51	352.22	101.3	78.13	35.70	26.88	20.73	14.65	9.48	6.01	7.55	6.75	7.29	44.10	577.72	115.03	39.80	17.47	12.76	9.34	10.03	10.98	8.31	10.26
Sm	21.48	130.95	25.99	19.28	7.54	5.75	4.32	2.64	1.67	1.12	1.27	1.24	1.39	11.72	204.95	28.86	9.05	3.42	2.68	2.06	2.00	2.31	1.70	2.19
Eu	4.89	33.52	6.09	4.56	1.74	1.27	1.04	0.62	0.37	0.25	0.32	0.27	0.34	3.55	56.28	7.31	2.43	0.88	0.66	0.55	0.54	0.53	0.45	0.49
Gd	15.21	116.51	22.15	16.04	6.63	4.82	3.99	2.53	1.70	1.01	1.23	1.06	1.30	14.70	192.08	24.81	8.84	3.49	2.66	2.15	2.09	2.42	1.81	1.86
Tb	2.26	19.12	3.60	2.79	1.25	0.82	0.66	0.38	0.25	0.16	0.16	0.15	0.20	1.94	26.12	3.43	1.22	0.45	0.34	0.26	0.25	0.28	0.19	0.27
Dy	10.05	105.33	20.87	16.12	7.16	4.56	4.04	2.22	1.20	0.70	0.79	0.63	1.03	11.05	141.21	19.03	6.91	2.40	2.12	1.37	1.28	1.47	1.00	1.38
Ho	1.69	20.69	3.84	3.02	1.43	0.97	0.83	0.44	0.26	0.13	0.15	0.13	0.19	1.95	24.38	3.35	1.23	0.43	0.40	0.26	0.25	0.24	0.18	0.27
Er	4.28	52.45	10.22	8.27	3.84	2.68	2.27	1.21	0.76	0.46	0.48	0.37	0.58	4.40	62.29	8.46	3.17	1.13	1.07	0.65	0.65	0.64	0.50	0.65
Tm	0.53	8.16	1.63	1.39	0.63	0.41	0.37	0.19	0.12	0.05	0.07	0.05	0.08	0.62	10.39	1.35	0.52	0.17	0.16	0.10	0.10	0.11	0.06	0.09
Yb	3.13	46.10	9.53	8.36	3.81	2.58	2.11	1.08	0.57	0.30	0.38	0.24	0.45	3.65	63.53	8.69	3.44	1.01	0.93	0.60	0.58	0.61	0.44	0.58
Lu	0.50	7.42	1.40	1.25	0.54	0.38	0.31	0.18	0.10	0.06	0.05	0.04	0.07	0.52	10.18	1.35	0.50	0.15	0.14	0.10	0.11	0.09	0.07	0.10
Y	15.51	155.65	47.00	35.93	21.37	15.67	12.29	8.31	4.89	2.88	3.06	2.74	4.25	18.85	137.40	33.67	15.90	8.97	6.96	5.30	5.07	6.20	4.19	6.12
ΣREE	247.32	1360.39	419.74	392.83	200.40	175.69	180.40	120.58	90.98	57.82	67.83	68.30	81.08	168.00	2236.61	449.94	246.74	155.30	95.24	82.95	103.1	106.52	83.01	73.71
REE-Ce	243.14	1292.25	354.05	278.36	139.64	105.09	83.77	60.64	39.24	23.92	27.98	24.35	28.5	160.62	2154.53	370.73	144.77	66.97	49.64	36.13	36.60	41.25	30.24	38.78
ΣLREE	194.16	828.97	299.49	299.67	153.74	142.81	153.52	104.03	81.13	52.07	61.46	62.90	72.92	110.32	1569.03	345.82	205.02	137.09	80.46	72.17	92.73	94.47	74.55	62.40
ΣHREE	53.16	531.42	120.24	93.17	46.66	32.88	26.87	16.54	9.84	5.75	6.37	5.40	8.16	57.67	667.58	104.12	41.72	18.21	14.78	10.78	10.37	12.05	8.46	11.32
ΣLREE/ΣHREE	3.65	1.56	2.49	3.22	3.29	4.34	5.71	6.29	8.24	9.06	9.65	11.64	8.94	1.91	2.35	3.32	4.91	7.53	5.44	6.69	8.94	7.84	8.82	5.51
LREE%	0.79	0.61	0.71	0.76	0.77	0.81	0.85	0.86	0.89	0.90	0.91	0.92	0.90	0.66	0.70	0.77	0.83	0.88	0.84	0.87	0.90	0.89	0.90	0.85
HREE%	0.21	0.39	0.29	0.24	0.23	0.19	0.15	0.14	0.11	0.10	0.09	0.08	0.10	0.34	0.30	0.23	0.17	0.12	0.16	0.13	0.10	0.11	0.10	0.15
δEu	0.83	0.83	0.78	0.79	0.75	0.74	0.76	0.73	0.68	0.71	0.79	0.71	0.77	0.83	0.87	0.84	0.83	0.78	0.75	0.80	0.80	0.68	0.79	0.75
δCe	0.03	0.14	0.36	0.76	0.75	1.12	1.92	1.48	1.89	2.01	2.05	2.56	2.86	0.10	0.07	0.38	1.16	2.09	1.52	2.21	2.97	2.61	2.85	1.48
$(La/Yb)_N$	12.15	2.36	5.26	5.03	6.72	8.06	7.96	13.67	17.65	20.16	18.39	25.02	13.68	6.12	5.28	6.73	8.01	14.83	11.16	12.41	12.87	13.74	13.90	13.68
$(La/Sm)_N$	1.65	0.77	1.80	2.04	3.17	3.37	3.63	5.20	5.63	5.03	5.10	4.44	4.18	1.78	1.53	1.89	2.84	4.09	3.62	3.37	3.48	3.40	3.39	3.40
$(Gd/Yb)_N$	3.92	2.04	1.88	1.55	1.40	1.51	1.53	1.90	2.40	2.71	2.61	3.64	2.31	3.25	2.44	2.30	2.07	2.79	2.31	2.89	2.92	3.19	3.29	2.58

All concentrations are normalized to the bulk sample and given in ppm.
The Ce anomaly($\delta Ce = Ce_N/[(La_N + Pr_N)/2]$)were calculated.
Listed also the $(La/Yb)_N = ((La/La_N)/(Yb/Yb_N))$, $(La/Sm)_N = ((La/La_N)/(Sm/Sm_N))$and $(Gd/Yb)_N = ((Gd/Gd_N)/(Yb/Yb_N))$ ratios indicating the degree of REE.

Table 4
The Al, Fe, Mn contents and TOC, pH from Qingzhen profile.

Sample	QZ-01	QZ-02	QZ-03	QZ-04	QZ-05	QZ-06	QZ-07	QZ-08	QZ-09	QZ-10	QZ-11	QZ-12	QZ-13	QZ-14	QZ-15	QZ-16	QZ-17	QZ-18	QZ-19	QZ-20	QZ-21	QZ-22	QZ-23	QZ-24	QZ-25
Depth (m)			5.55	5.3	5.05	4.80	4.55	4.30	4.05	3.80	3.55	3.30	3.05	2.80	2.55	2.30	2.05	1.80	1.55	1.30	1.05	0.80	0.55	0.30	0.05
Th (ppm)	0.17	0.09	0.50	22.70	30.60	28.00	14.90	32.70	30.50	30.30	32.20	33.20	32.40	28.60	33.30	35.10	35.20	34.60	35.90	22.40	30.70	31.30	29.20	24.40	26.10
Al	0.02	0.04	0.21	12.37	16.29	15.90	8.83	17.74	17.06	16.66	16.99	17.06	16.89	14.89	16.72	17.85	17.63	16.66	17.31	12.28	14.62	13.96	12.25	8.97	10.80
Fe	0.09	0.02	0.22	7.53	8.84	8.32	5.56	7.95	8.94	9.62	9.56	9.27	9.28	8.74	8.32	9.10	9.58	9.85	9.95	21.33	10.60	8.36	7.68	5.35	6.75
Mn	0.02	0.02	0.01	0.10	0.08	0.09	0.09	0.13	0.09	0.07	0.09	0.09	0.10	0.17	0.09	0.07	0.07	0.09	0.28	0.17	0.07	0.06	0.11	0.15	0.08
TOC (%)			6.15	0.38	0.33	0.33	0.19	0.35	0.31	0.31	0.31	0.31	0.30	0.31	0.30	0.34	0.31	0.32	0.30	0.32	0.41	0.37	0.41	0.94	2.65
pH			8.44	6.64	6.53	6.48	6.29	6.07	5.56	5.17	4.94	4.81	5.06	5.05	4.89	4.87	4.71	4.58	4.48	4.54	4.47	4.46	5.22	5.31	5.04
Al (leachate)		−0.02	0.06	1.49	1.68	1.32	0.95	1.75	1.79	1.68	1.59	1.54	1.68	1.76	1.56	1.48	1.58	1.48	1.51	1.20	1.43	1.46	1.51	1.57	1.88
Fe (leachate)		0.02	0.07	1.71	1.66	1.53	1.38	1.75	1.96	1.82	1.71	1.63	1.70	1.94	1.56	1.53	1.66	1.60	1.75	5.42	1.73	1.40	1.55	1.36	1.44
Mn (leachate)		0.00	0.01	0.07	0.05	0.06	0.08	0.09	0.06	0.05	0.05	0.05	0.06	0.13	0.05	0.03	0.04	0.05	0.18	0.11	0.03	0.03	0.08	0.12	0.06

Major elements are given in oxide mass percentage (%).

Table 5
The Al, Fe, Mn contents and TOC, pH from Pingba profile.

Sample	HY	PB-3	PB-4	PB-5	PB-6	PB-7	PB-8	PB-9	PB-10	PB-11	PB-12	PB-13	PB-14	PB-15	PB-16	PB-17	PB-18	PB-19	PB-20	PB-21	PB-22
Depth (m)	7.25	4.80	4.55	4.30	4.05	3.80	3.55	3.30	3.05	2.80	2.55	2.30	2.05	1.80	1.55	1.30	1.05	0.80	0.55	0.30	0.05
Th (ppm)	0.24	1.42	29.20	30.00	29.80	29.90	29.50	26.50	25.40	23.40	29.00	31.10	32.70	33.70	33.10	31.80	32.20	32.60	29.40	24.70	22.70
Al	0.09	0.76	15.55	15.92	15.59	15.62	15.26	14.87	16.14	12.43	14.19	16.24	15.29	15.43	15.67	15.61	16.14	16.10	14.45	10.70	9.55
Fe	0.13	0.53	9.23	9.02	9.34	9.09	9.48	9.30	10.53	8.46	10.23	12.63	10.50	9.98	9.88	9.89	10.86	10.95	9.36	6.22	6.14
Mn	0.005	0.01	0.15	0.14	0.13	0.08	0.16	0.14	0.12	0.03	0.03	0.04	0.03	0.03	0.03	0.03	0.03	0.03	0.03	0.04	0.06
TOC (%)		6.86	0.59	0.52	0.52	0.38	0.38	0.29	0.23	0.26	0.33	0.39	0.44	0.41	0.45	0.50	0.59	0.75	0.85	0.75	2.09
pH		7.02	5.96	5.72	5.68	5.49	5.42	5.28	5.23	5.19	5	5	5.13	5.06	4.91	5	4.9	4.84	4.67	4.79	5.74
A l(leachate)		0.27	2.44	2.20	1.96	1.88	2.06	1.86	2.12	1.37	1.75	1.69	1.81	1.90	1.79	1.75	1.76	1.74	1.82	1.73	1.87
Fe (leachate)		0.20	2.75	2.62	2.55	2.43	2.52	2.26	1.71	1.85	2.48	2.62	3.22	2.68	2.25	2.08	2.29	2.22	1.99	1.36	1.63
Mn (leachate)		0.01	0.13	0.11	0.10	0.06	0.13	0.09	0.07	0.02	0.02	0.02	0.02	0.01	0.01	0.01	0.01	0.01	0.01	0.02	0.04

Major elements are given in oxide mass percentage (%).

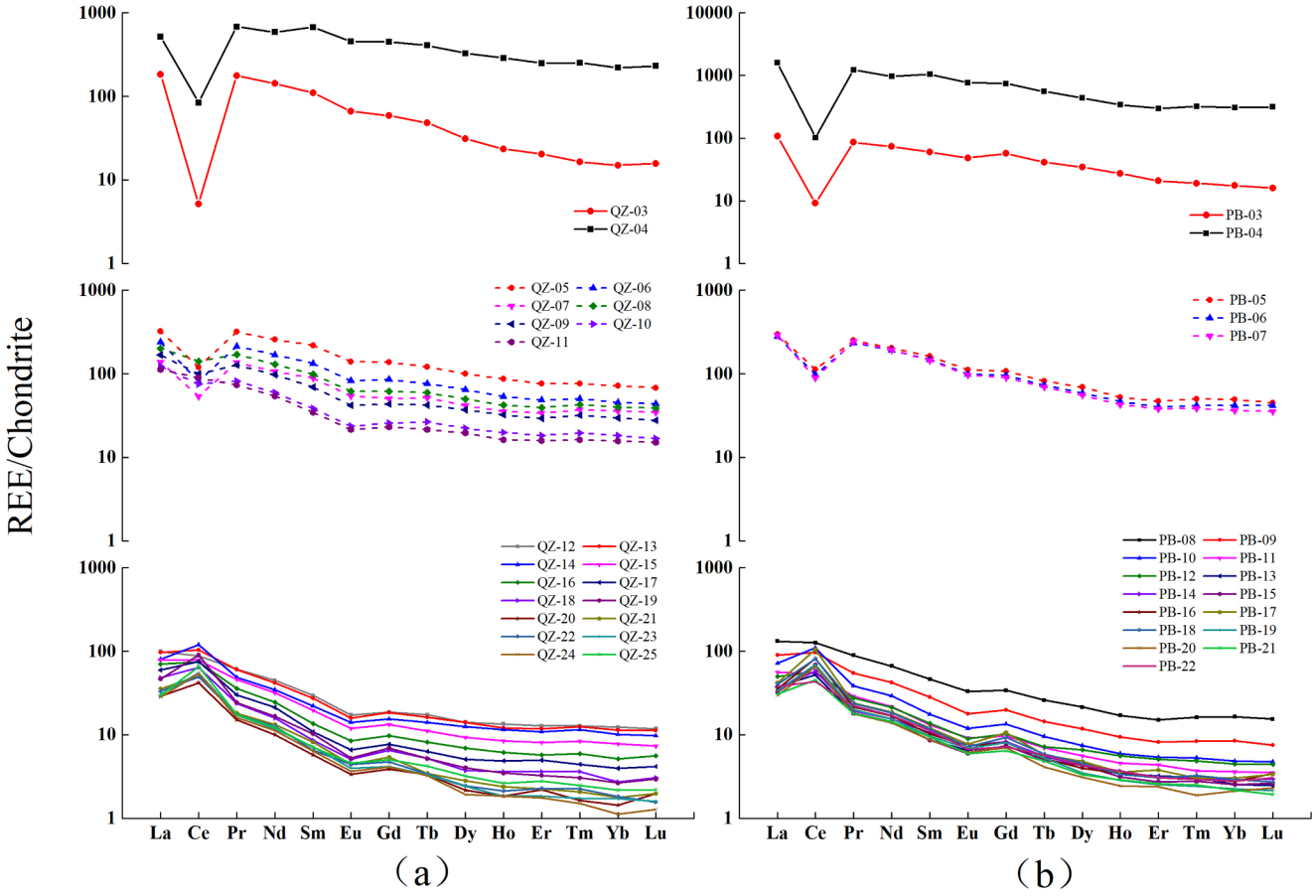

Fig. 6. Chondrite-normalized REE patterns of leachates from Qingzhen profile (a) and Pingba profile (b).

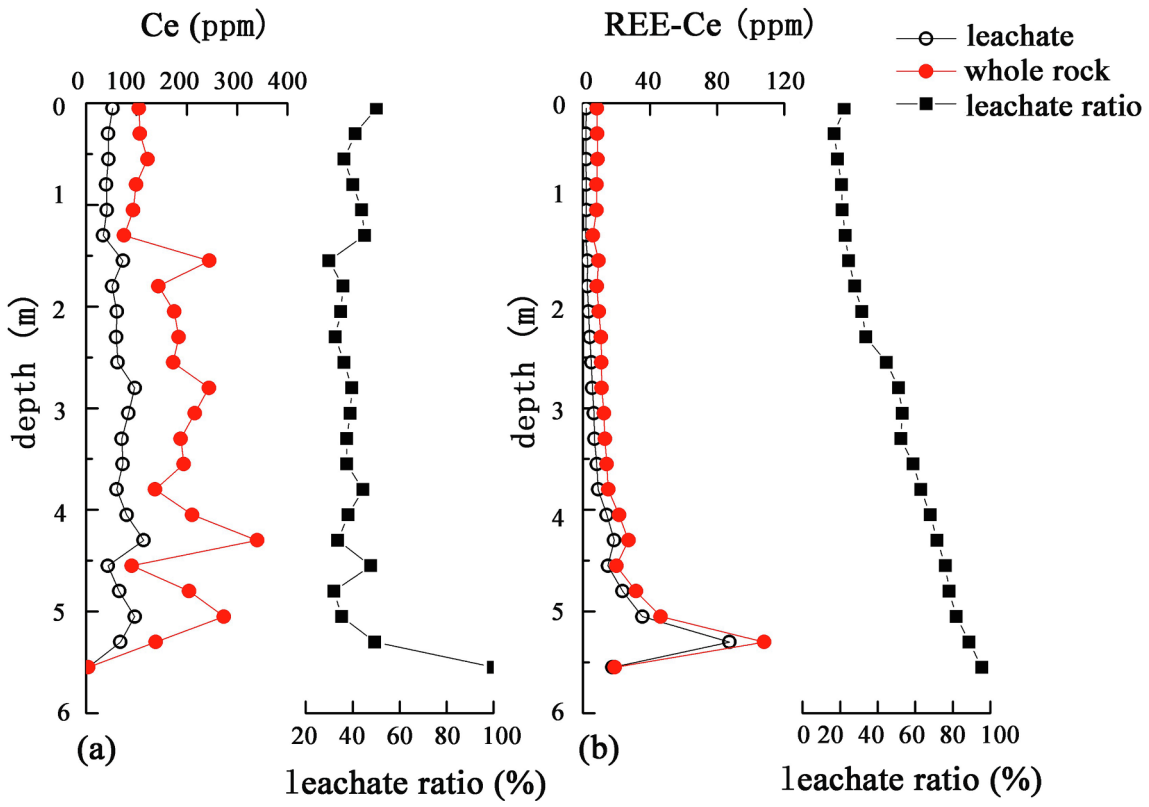

Fig. 7. In-depth variations of the concentrations in leachates, whole rock samples and leachate ratio changes of Ce and REE-Ce from Qingzhen profile (a) and (b), respectively.

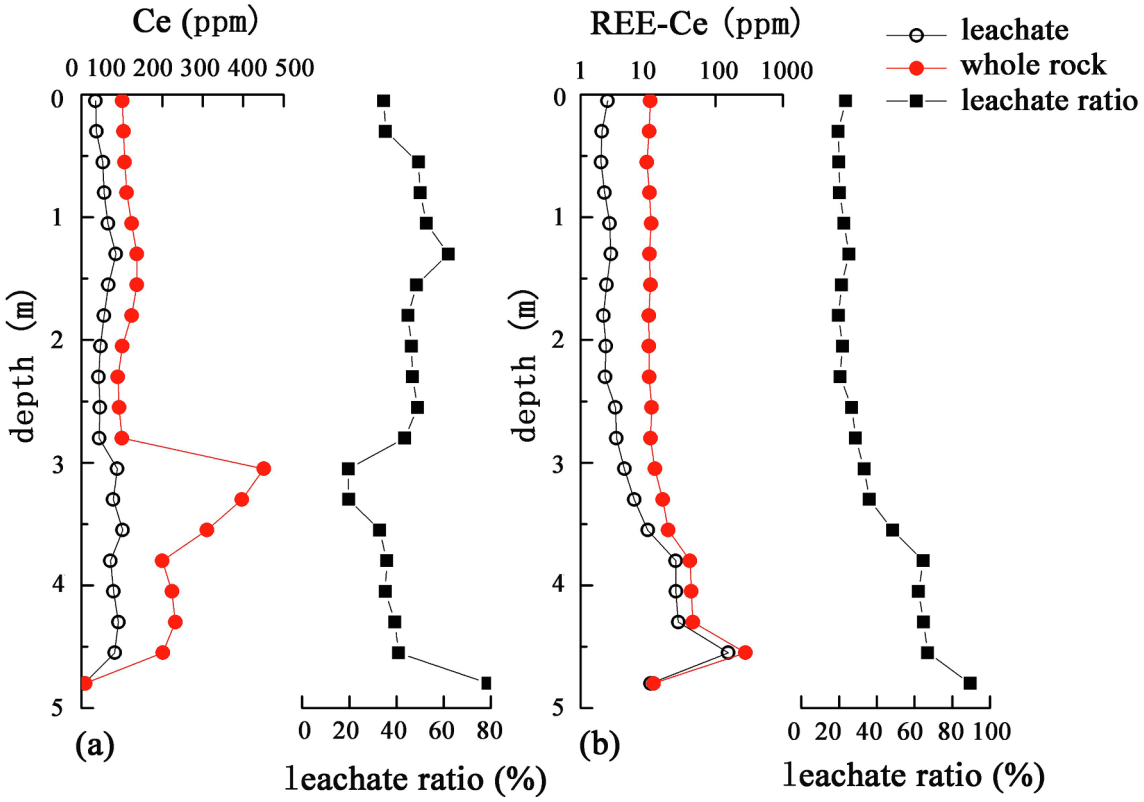

Fig. 8. In-depth variations of the concentrations in leachates, whole rock samples and leachate ratio changes of Ce and REE-Ce from Pingba (a) and (b), respectively.

This finding further verifies that weathering crust has the characteristics of in situ weathering and inherits the underlying dolomite. Previous studies stated that aqueous REE characteristics are inherited from underlying bedrock REEs during weathering process (Lev and Filer, 2004; Jin et al., 2017; Ma et al., 2011; Yusoff et al., 2013). A similar pattern is observed in leachates and soils of QZ and PB profiles. The red soil that developed on carbonate rocks undergoes a large volumetric change in the rock–soil interface, causing elemental enrichment in this layer. This phenomenon also explains that the red weathering crust is derived from the parent rock through long-term weathering.

From bottom to top, the two profiles, including the bedrock, rock powder layer, regolith, ferruginous crust, and surface soil layer,

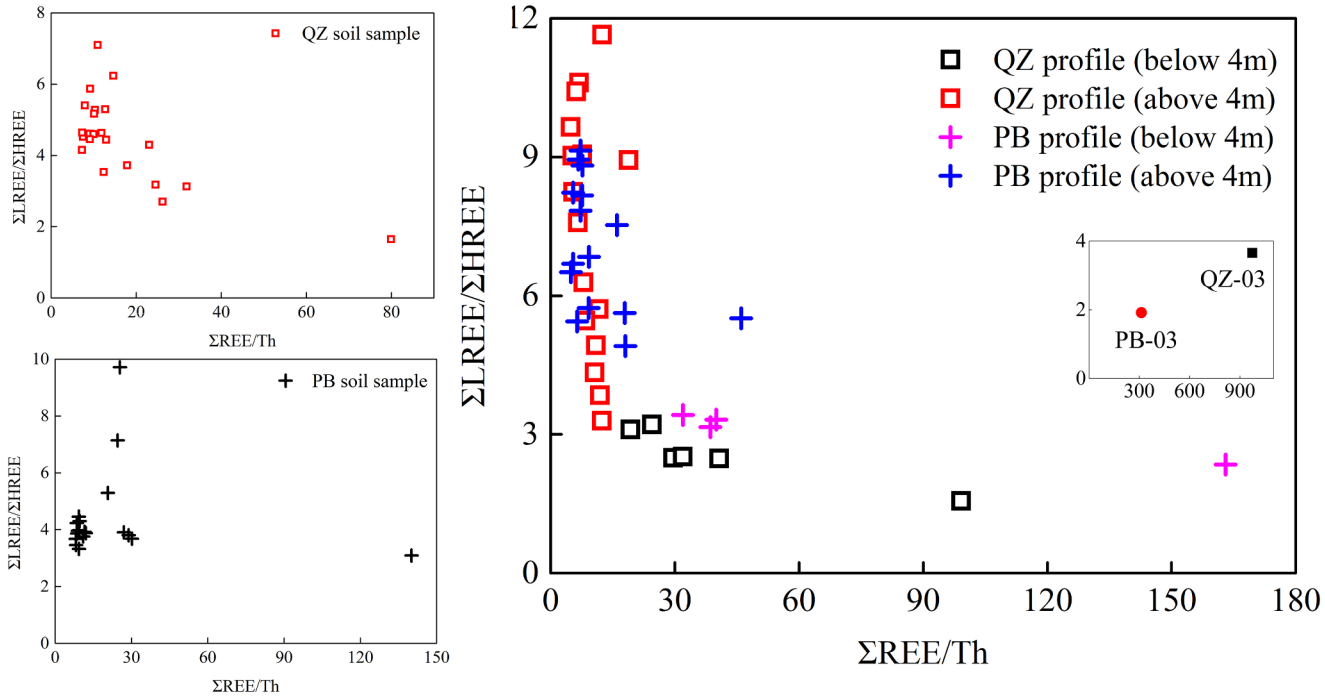

Fig. 9. LREE/HREE ratios *vs.* ΣREE/Th ratios in leachates and soil samples in Qingzhen and Pingba profiles. The arrow indicates the pedogenesis and weathering trend.

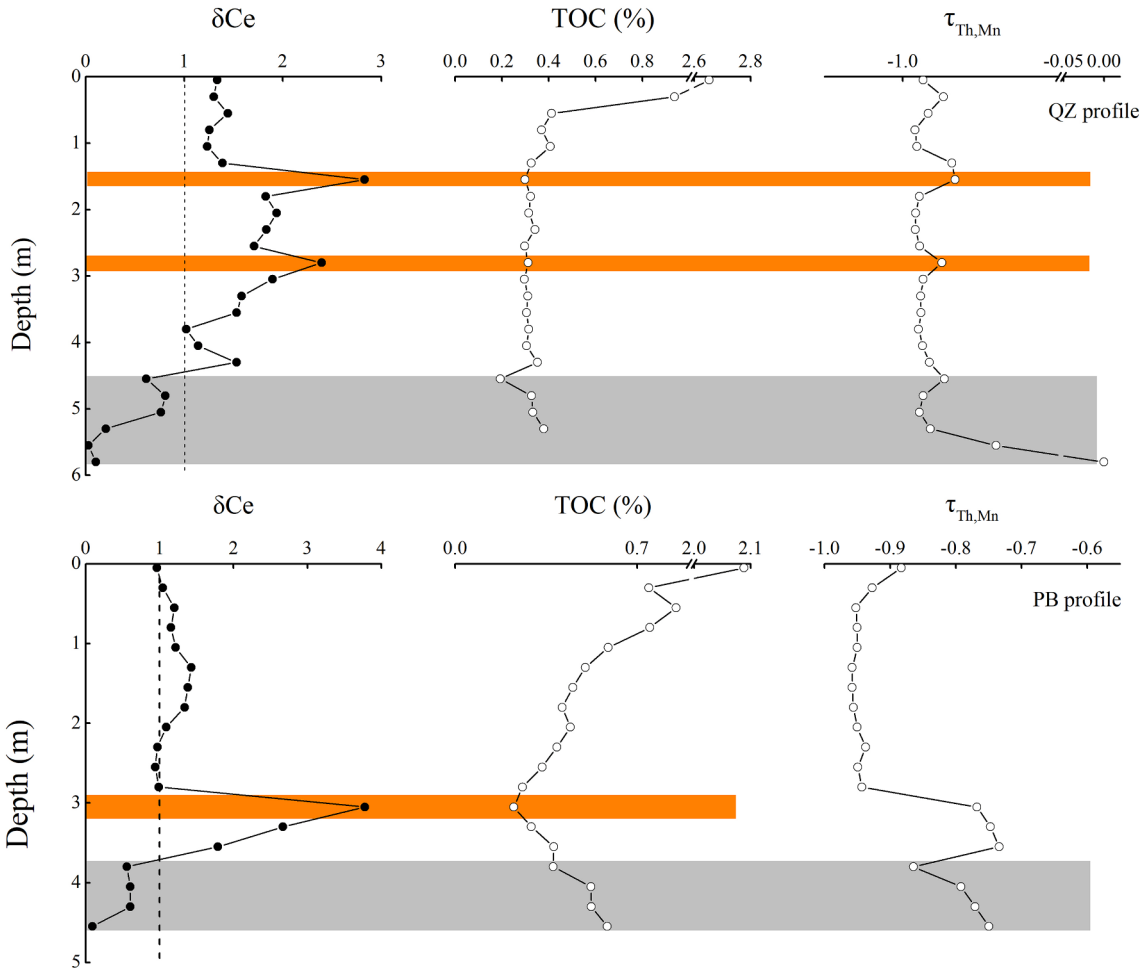

Fig. 10. Depth variations of Ce anomaly, TOC contents and $\tau_{Th,Mn}$ in Qingzhen and Pingba profiles.

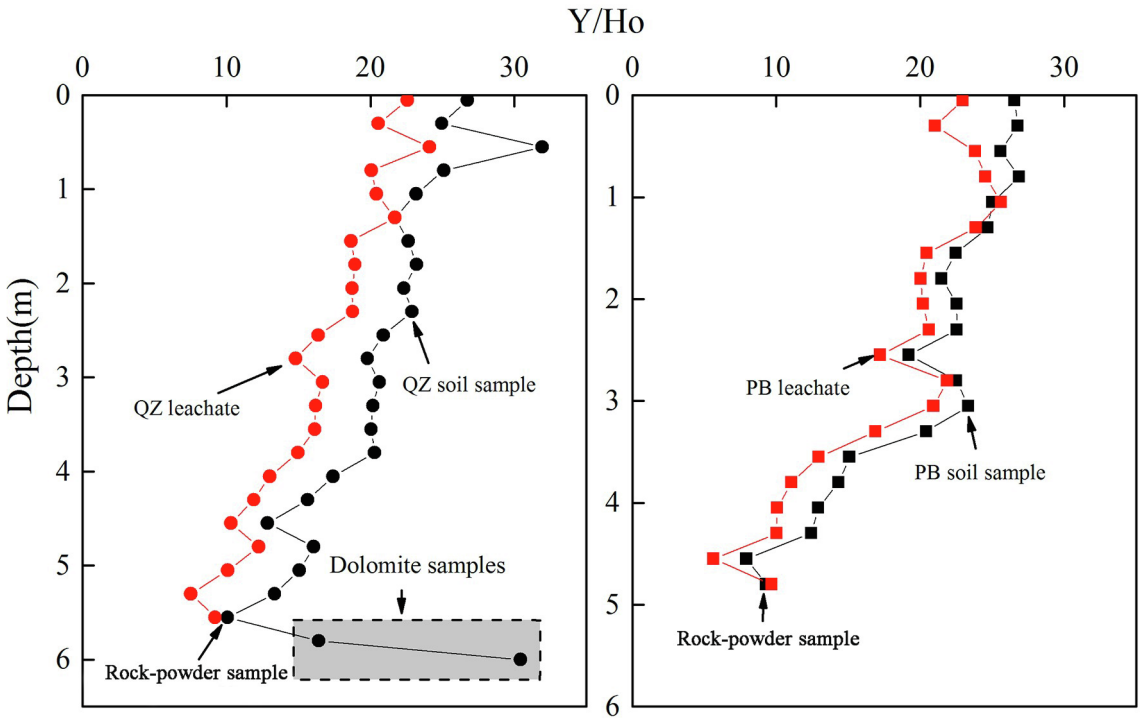

Fig. 11. Correlations between Y and Ho concentrations in leachates and soil samples of Qingzhen profile (a) and Pingba profile (b).

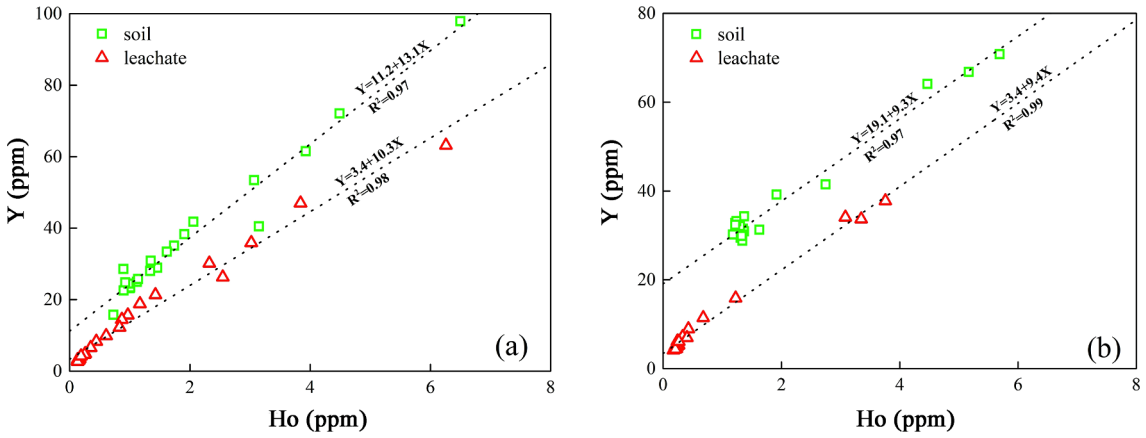

Fig. 12. Depth variations of Y/Ho weight ratios in leachates and soil samples in Qingzhen and Pingba profiles.

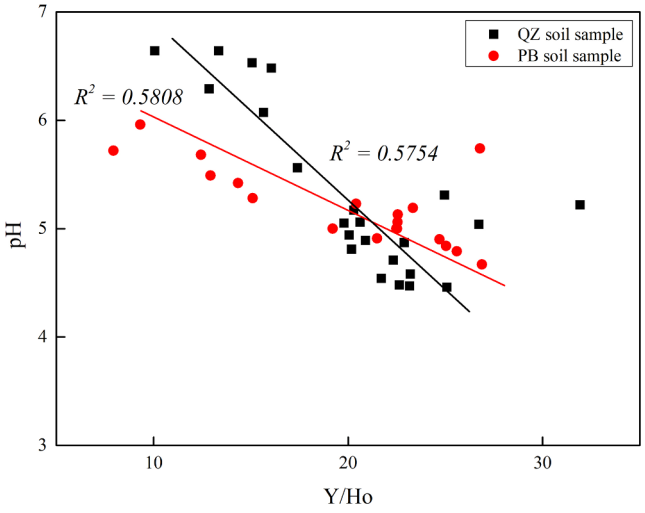

Fig. 13. The pH *vs.* Y/Ho ratios in in Qingzhen and Pingba profiles.

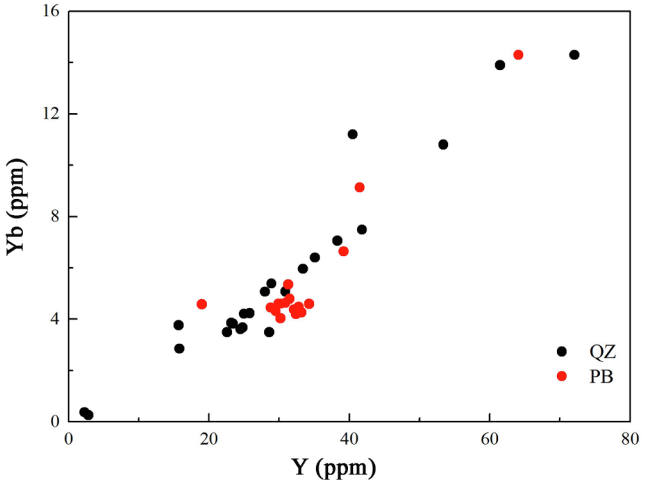

Fig. 14. Correlations between Y and Yb concentrations in soil samples of in Qingzhen and Pingba profiles.

constitute a complete profile with in situ weathering characteristics (Wang et al., 1999). The ferruginous crust can provide evidence that the profiles have in situ leaching–weathering profiles (Nahon, 1986; Tardy et al., 1991). During field observation, the soil layers on different rocks have obvious differences, and a certain relationship between soil layers and underlying bedrock can be preliminarily determined (Li et al., 1991). The laterite developed by carbonate rocks undergoes tremendous non-isovolumetric shrinkage at the rock–soil interface, resulting in the enrichment of elements (Ji et al., 2004a, b). This finding also confirms that red weathering crust is derived from the parent rock after long-term weathering. Based on data analysis, the studied soil profiles have the characteristics of in situ weathering. The present study has considerable research importance on REE behavior in soils overlying dolomite and on provenance analysis of residual soil in the karst area.

5. Conclusion

By investigating REE behavior in lateritic weathering crust through HCl experiment to leach soil samples and by comparing the REE contents in leachates and bulk samples, the following major conclusions are drawn:

(1) ΣREE decreases from the bottom to the upper layers of the profile, indicating that REE mobilization is mainly affected by leaching. pH and TOC play an important role in REE mobility and redistribution. Meanwhile, high LREE/HREE and $(La/Yb)_N$ ratios verify that LREEs are more mobile than HREEs during pedogenesis.
(2) The large Ce anomalies in chondrite-normalized REE distribution patterns exhibit negative and positive Ce anomalies in the lower and upper parts of the profiles, respectively. This phenomenon is also observed in the leachates, indicating that the anomaly is affected by parent carbonates and redox environment. Therefore, the basic properties and behavior of the element must be considered when using Ce as tracer to indicate the redox environment in the weathering process.
(3) The similar Y/Ho trends of leachates and bulk samples indicate a slight or low fractionation for Y and Ho during acid leaching. From the LREE/HREE and ΣREE/Th values in leachates, considerable weathering and pedogenetic trends are observed under acidic leaching environment.
(4) According to elemental change and Y/Yb ratio, the studied profiles have the characteristics of in situ weathering.

Declaration of Competing Interest

The authors declare that they have no known competing financial interests or personal relationships that could have appeared to influence the work reported in this paper.

Acknowledgements

We thank Ms. Li Zhang for her assistance with field sampling and analysis. The work was supported by the National Natural Science Foundation of China (NSFC) grants (41473122, 41073096), the

National Key Basic Research Program of China (2013CB956702) and the Hundred Talents Program of the Chinese Academy of Sciences.

Appendix A. Supplementary material

Supplementary data to this article can be found online at https://doi.org/10.1016/j.jseaes.2019.104023.

References

Aja, S.U., 1998. The sorption of the rare earth element, Nd, onto kaolinite at 25°C. Clays Clay Miner. 46, 103–109.

Anderson, S.P., Dietrich, W.E., Brimhall, G.H., 2002. Weathering profiles, mass-balance analysis, and rates of solute loss: Linkages between weathering and erosion in a small, steep catchment. GSA Bull. 114, 1143–1158.

Balashov, Y.A., Girin, Y.P., 1969. On the reserve of mobile rare earth elements in sediment rocks. Geochem. Int. 7, 649–658.

Banfield, J., Eggleton, R., 1989. Apatite replacement and rare earth mobilization, factionation, and fxation dring wathering. Clays Clay Miner. 37, 113–127.

Bau, M., 1999. Scavenging of dissolved yttrium and rare earths by precipitating iron oxyhydroxide; experimental evidence for Ce oxidation, Y-Ho fractionation, and lanthanide tetrad effect. Geochim. Cosmochim. Acta 63, 67–77.

Bau, M., Dulski, P., 1995. Comparative study of yttrium and rare-earth behaviors in fluorine-rich hydrothermal fluids. Contrib. Mineral. Petr. 119, 213–223.

Bau, M., Möller, P., Dulski, P., 1997. Yttrium and lanthanides in eastern Mediterranean seawater and their fractionation during redox-cycling. Mar. Chem. 56, 123–131.

Berger, A., Janots, E., Gnos, E., Frei, R., Bernier, F., 2014. Rare earth element mineralogy and geochemistry in a laterite profile from Madagascar. Appl. Geochem. 41, 218–228.

Boulangé, B., Colin, F., 1994. Rare earth element mobility during conversion of nepheline syenite into lateritic bauxite at Passa Quatro, Minais Gerais, Brazil. Appl. Geochem. 9, 701–711.

Braun, J.J., Pagel, M., Herbillon, A., Rosin, C., 1993. Mobilization and redistribution of REEs and thorium in a syenitic lateritic profile; a mass balance study. Geochim. Cosmochim. Acta 57, 4419–4434.

Braun, J.J., Pagel, M., Muller, J.-P., Bilong, P., Michard, A., Guillet, B., 1990. Cerium anomalies in lateritic profiles. Geochim. Cosmochim. Acta 54, 781–795.

Braun, J.J., Riotte, J., Battacharya, S., Violette, A., Oliva, P., Prunier, J., Marechal, J.C., Ruiz, L., Audry, S., Subramanian, S., 2018. REY-Th-U Dynamics in the critical zone: combined influence of reactive bedrock accessory minerals, Authigenic phases, and hydrological sorting (Mule Hole Watershed, South India). Geochem. Geophy. Geosy. 19, 1611–1635.

Braun, J.J., Riotte, J., Battacharya, S., Violette, A., Prunier, J., Bouvier, V., Candaudap, F., Marechal, J.C., Ruiz, L., Panda, S.R., Subramanian, S., 2017. REY-Th-U solute dynamics in the critical zone: combined influence of chemical weathering, atmospheric deposit leaching, and vegetation cycling (Mule Hole Watershed, South India). Geochem. Geophy. Geosy. 18, 4409–4425.

Braun, J.J., Viers, J., Dupré, B., Polve, M., Ndam, J., Muller, J.-P., 1998. Solid/liquid REE fractionation in the lateritic system of Goyoum, East Cameroon: the implication for the present dynamics of the soil covers of the humid tropical regions. Geochim. Cosmochim. Acta 62, 273–299.

Brimhall, G., Dietrich, W., 1987. Constitutive mass balance relations between chemical composition, volume, density, porosity, and strain in metasomatic hydrochemical systems: Results on weathering and pedogenesis. Geochim. Cosmochim. Acta 51, 567–587.

Cao, X., Chen, Y., Wang, X., Deng, X., 2001. Effects of redox potential and pH value on the release of rare earth elements from soil. Chemosphere 44, 655–661.

Censi, P., Sprovieri, M., Saiano, F., Di Geronimo, S., Larocca, D., Placenti, F., 2007. The behaviour of REEs in Thailand's Mae Klong estuary: Suggestions from the Y/Ho ratios and lanthanide tetrad effects. Estuar. Coast. Shelf. S. 71, 569–579.

Coppin, F., Berger, G., Bauer, A., Castet, S., Loubet, M., 2002. Sorption of lanthanides on smectite and kaolinite. Chem. Ceol. 182, 57–68.

De Carlo, E.H., Wen, X.Y., Irving, M., 1998. The influence of redox reactions on the uptake of dissolved Ce by suspended Fe and Mn oxide particles. Aquat. Geochem. 3, 357–389.

da Silva, Y.J.A.B., Do Nascimento, C.W.A., Biondi, C.M., van Straaten, P., de Souza Júnior, V.S., da Silva, Y.J.A.B., dos Santos, C.A., do Carmo Trezena de Araújo, J., 2017. Influence of metaluminous granite mineralogy on the rare earth element geochemistry of rocks and soils along a climosequence in Brazil. Geoderma 306, 28–39.

De Baar, H.J.W., German, C.R., Elderfield, H., Gaans, P.V., 1988. Rare earth element distributions in anoxic waters of the Cariaco Trench. Geochim. Cosmochim. Acta 52, 1203–1219.

Dou, Y., Yang, S., Liu, Z., Clift, P.D., Shi, X., Yu, H., Berne, S., 2010. Provenance discrimination of siliciclastic sediments in the middle Okinawa Trough since 30 ka: constraints from rare earth element compositions. Mari. Geol. 275, 212–220.

Du, X., Rate, A.W., Gee, M.A.M., 2012. Redistribution and mobilization of titanium, zirconium and thorium in an intensely weathered lateritic profile in Western Australia. Chem. Ceol. 330–331, 101–115.

Duddy, L.R., 1980. Redistribution and fractionation of rare-earth and other elements in a weathering profile. Chem. Ceol. 30, 363–381.

Feng, J.L., 2010. Behavior of rare earth elements and yttrium in ferromanganese concretions, gibbsite spots, and the surrounding terra rossa over dolomite during chemical weathering. Chem. Ceol. 271, 112–132.

Feng, J.L., Cui, Z.J., Zhu, L.P., 2009. Origin of terra rossa over dolomite on the Yunnan-Guizhou Plateau. China. Geochem. J. 43 (3), 151–166.

Galán, E., Fernández-Caliani, J.C., Miras, A., Aparicio, P., Márquez, M.G., 2007. Residence and fractionation of rare earth elements during kaolinization of alkaline peraluminous granites in NW Spain. Clay Miner. 42, 341–352.

Hill, I., Worden, R., Meighan, I., 2000. Yttrium: the immobility-mobility transition during basaltic weathering. Geology 28, 923–926.

Janots, E., Bernier, F., Brunet, F., Muñoz, M., Trcera, N., Berger, A., Lanson, M., 2015. Ce (III) and Ce(IV) (re)distribution and fractionation in a laterite profile from Madagascar: Insights from in situ XANES spectroscopy at the Ce LIII -edge. Geochim. Cosmochim. Acta 153, 134–148.

Ji, H.B., Wang, S.J., Ouyang, Z.Y., Zhang, S., Sun, C., Liu, X., Zhou, D., 2004a. Geochemistry of red residua underlying dolomites in karst terrains of Yunnan-Guizhou Plateau: I. The formation of the Pingba profile. Chem. Ceol. 203, 29–50.

Ji, H.B., Wang, S.J., Ouyang, Z.Y., Zhang, S., Sun, C., Liu, X., Zhou, D., 2004b. Geochemistry of red residua underlying dolomites in karst terrains of Yunnan-Guizhou Plateau:II. The mobility of rare earth elements during weathering. Chem. Ceol. 203, 1–27.

Jin, L.X., Ma, L., Dere, A., White, T., Mathur, R., Brantley, S.L., 2017. REE mobility and fractionation during shale weathering along a climate gradient. Chem. Ceol. 466, 352–379.

Jung, H.S., Lim, D., Choi, J.Y., Yoo, H.S., Rho, K.C., Lee, H.B., 2012. Rare earth element compositions of core sediments from the shelf of the South Sea, Korea: their controls and origins. Cont. Shelf Res. 48, 75–86.

Jung, H.S., Lim, D., Jeong, D.H., Xu, Z., Li, T., 2016. Discrimination of sediment provenance in the Yellow Sea: Secondary grain-size effect and REE proxy. J. Asian Earth Sci. 123, 78–84.

Kanazawa, Y., Kamitani, M., 2006. Rare earth minerals and resources in the world. J Alloy. Compd. 408–412, 1339–1343.

Kuss, J., Garbe Schönberg, C.D., Kremling, K., 2001. Rare earth elements in suspended particulate material of North Atlantic surface waters. Geochim. Cosmochim. Acta 65, 187–199.

Laveuf, C., Cornu, S., 2009. A review on the potentiality of Rare Earth Elements to trace pedogenetic processes. Geoderma 154, 1–12.

Laveuf, C., Cornu, S., Guilherme, L., Guerin, A., Juillot, F., 2012. The impact of redox conditions on the rare earth element signature of redoximorphic features in a soil sequence developed from limestone. Geoderma 170, 25–38.

Leleyter, L., Probst, J.L., Depetris, P., Haida, S., Mortatti, J., Rouault, R., Samuel, J., 1999. REE distribution pattern in river sediments: partitioning into residual and labile fractions. Earth Planet. Sci. 329, 45–52.

Lev, S.M., Filer, J.K., 2004. Assessing the impact of black shale processes on REE and the U-Pb isotope system in the southern Appalachian Basin. Chem. Ceol. 206, 393–406.

Leybourne, M.I., Johannesson, K.H., 2008. Rare earth elements (REE) and yttrium in stream waters, stream sediments, and Fe–Mn oxyhydroxides: Fractionation, speciation, and controls over REE + Y patterns in the surface environment. Geochim. Cosmochim. Acta 72, 5962–5983.

Li, M.Y.H., Wen, W.Z., Zhou, M.F., 2017. Nature of parent rocks, mineralization styles and ore genesis of regolith-hosted REE deposits in South China: An integrated genetic model. J. Asian Earth Sci. 148, 65–95.

Li, M.Y.H., Zhou, M.F., Williams-Jones, A.E., 2019. The genesis of regolith-hosted HREE deposits: Insights from the world-class Zudong deposit in Jiangxi Province, South China. Eco. Geol. 114, 541–568.

Li, J., Wang, C., Fan, T., 1991. Weathering crust of carbonate rocks and process of karst earth formation. Carsol Sinica 10 (1), 29–38 (in Chinese with English abstract).

Ma, J.L., Wei, G.J., Xu, Y.G., 2007a. Relationship between REE and Al, P, Fe and Mn in basaltic weathering products: Evidences from hydrochloric acid leaching. Geochemica 36, 633–637 (in Chinese with English abstract).

Ma, J.L., Wei, G.J., Xu, Y.G., Long, W.G., Sun, W.D., 2007b. Mobilization and re-distribution of major and trace elements during extreme weathering of basalt in Hainan Island, South China. Geochim. Cosmochim. Acta 71, 3223–3237.

Ma, L., Jin, L., Brantley, S.L., 2011. How mineralogy and slope aspect affect REE release and fractionation during shale weathering in the Susquehanna/Shale Hills Critical Zone Observatory. Chem. Ceol. 290, 31–49.

Marsh, J.S., 1991. REE fractionation and Ce anomalies in weathered Karoo dolerite. Chem. Ceol. 90, 189–194.

McLennan, S.M., 1989. Rare earth elements in sedimentary rocks; influence of provenance and sedimentary processes. Rev. Mineral. Geochem. 21, 169–200.

Mongelli, G., 1993. REE and other trace elements in a granitic weathering profile from “Serre”, southern Italy. Chem. Ceol. 103, 17–25.

Nahon, D., 1986. Evolution of Iron Crusts in Tropical Landscapes. Rates of Chemical Weathering of Rocks and Minerals. Academic Press, New York, pp. 169–191.

Nahon, D., 2003. Weathering in tropical zone. Significance through ancient and still active mechanisms. Cr. Geosci. 335, 1109–1119.

Nakada, Ryoichi, Tanimizu, Takahashi, 2013. Isotopic and speciation study on cerium during its solid-water;distribution with implication for Ce stable isotope as a paleo-redox;proxy. Geochim. Cosmochim. Acta 103, 49–62.

Nasraoui, M., Toulkeridis, T., Clauer, N., Bilal, E., 2000. Differentiated hydrothermal and meteoric alterations of the Lueshe carbonatite complex (Democratic Republic of Congo) identified by a REE study combined with a sequential acid-leaching experiment. Chem. Ceol. 165, 109–132.

Nesbitt, H., Markovics, G., 1997. Weathering of granodioritic crust, long-term storage of elements in weathering profiles, and petrogenesis of siliciclastic sediments. Geochim. Cosmochim. Acta 61, 1653–1670.

Nesbitt, H.W., Markovics, G., 1980. Chemical processes affecting alkalis and alkaline earths during continental weathering. Geochim. Cosmochim. Acta 44, 1659–1666.

Ni, S., Yang, S., Guo, Y., Yue, W., Wang, X., Yin, P., Huang, X., 2017. Revisit of rare earth element fractionation during chemical weathering and river sediment transport. Geochem. Geophy. Geosy. 18, 935–955.
Nozaki, Y., Lerche, D., Alibo, D.S., Snidvongs, A., 2000. The estuarine geochemistry of rare earth elements and indium in the Chao Phraya River, Thailand. Geochim. Cosmochim. Acta 64, 3983–3994.
Nozaki, Y., Zhang, J., Amakawa, H., 1997. The fractionation between Y and Ho in the marine environment. Earth Planet. Sci. 148, 329–340.
Öhlander, B., Land, M., Ingri, J., Widerlund, A., 1996. Mobility of rare earth elements during weathering of till in northern Sweden. Appl. Geochem. 11, 93–99.
Ohta, A., Kawabe, I., 2001. REE(III) adsorption onto Mn dioxide (δ-MnO_2) and Fe oxyhydroxide: Ce(III) oxidation by δ-MnO_2. Geochim. Cosmochim. Acta 65, 695–703.
Palumbo, B., Bellanca, A., Neri, R., Roe, M., 2001. Trace metal partitioning in Fe–Mn nodules from Sicilian soils, Italy. Chem. Geol. 173, 257–269.
Parekh, P.P., Moller, P., Dulski, P., 1977. Distribution of trace elements between carbonate and non-carbonate phases of limestone. Earth Planet. Sci. Lett. 34, 39–50.
Patino, L.C., Velbel, M.A., Price, J.R., Wade, J.A., 2003. Trace element mobility during spheroidal weathering of basalts and andesites in Hawaii and Guatemala. Chem. Ceol. 202, 343–364.
Quinn, K.A., Byrne, R.H., Schijf, J., 2006. Sorption of yttriumand rare earth elements by amorphous ferric hydroxide: Influence of solution complexation with carbonate. Geochim. Cosmochim. Acta 70, 4151–4165.
Riebe, C.S., Hahm, W.J., Brantley, S.L., 2017. Controls on deep critical zone architecture: a historical review and four testable hypotheses. Earth Surf. Proc. Land. 42, 128–156.
Sholkovitz, E.R., 1989. Artifacts associated with the chemical leaching of sediments for rare-earth elements. Chem. Ceol. 77, 47–51.
Song, Y., Choi, M., 2009. REE geochemistry of fine-grained sediments from major rivers around the Yellow Sea. Chem. Ceol. 266, 328–342.
Sun, C.X., Wang, S.J., Ji, H.B., 2002. Formation mechanism of the superhigh concentration of REE and the strong negative Ce anomalies in the carbonate rock weathering profiles in Guizhou Province. China. Geochemica. 31, 119–128 (in Chinese with English abstract).
Tardy, Y., Kobilsek, B., Paquet, H., 1991. Mineralogical composition and geographical distribution of African and Brazilian periatlantic laterites. The influence of continental drift and tropical paleoclimates during the past 150 million years and implications for India and Australia. J. Asian Earth Sci. 12, 283–295.
Taunton, A., Welch, S., Banfield, J., 2000. Geomicrobiological controls on light rare earth element, Y and Ba distributions during granite weathering and soil formation. J. Alloy. Compd. 303–304, 30–36.
Taylor, S.R., McLennan, S.M., 1981. The composition and evolution of the continental crust: rare earth element evidence from sedimentary rocks. Phil. Trans. R. Soc. Lond. A 301, 381–399.
Taylor, S.R., McLennan, S.M., 1985. Continental Crust: Its Composition and Evolution. An Examination of the Geochemical Record Preserved in Sedimentary Rocks. Blackwell Scientific Publications.
Taylor, S.R., Rudnick, R.L., McLennan, S.M., Eriksson, K.A., 1986. Rare earth element patterns in Archean high-grade metasediments and their tectonic significance. Geochim. Cosmochim. Acta 50, 2267–2279.
Thompson, A., Amistadi, M.K., Chadwick, O.A., Chorover, J., 2013. Fractionation of yttrium and holmium during basaltic soil weathering. Geochim. Cosmochim. Acta 119, 18–30.
Vázquez-Ortega, A., Perdrial, J., Harpold, A., Zapata-Ríos, X., Rasmussen, C., McIntosh, J., Schaap, M., Pelletier, J., Brooks, P., Amistadi, M., Chorover, J., 2015. Rare earth elements as reactive tracers of biogeochemical weathering in forested rhyolitic terrain. Chem. Ceol. 391, 19–32.
Vermeire, M.L., Cornu, S., Fekiacova, Z., Detienne, M., Delvaux, B., Cornélis, J.-T., 2016. Rare earth elements dynamics along pedogenesis in a chronosequence of podzolic soils. Chem. Ceol. 163–174.
Wang, S.J., Ji, H.B., Ouyang, Z.Y., Zhou, D., Zhen, L., Li, T., 1999. Preliminary study on weathering and pedogenesis of carbonate rock. Sci. China, Ser. D Earth Sci. 42, 572–581 (in Chinese with English abstract).
Yang, S.Y., Jung, H.S., Choi, M.S., Li, C.X., 2002. The rare earth element compositions of the Changjiang (Yangtze) and Huanghe (Yellow) river sediments. Earth Planet. Sci. 201, 407–419.
Young, G.M., Nesbitt, H.W., 1998. Processes controlling the distribution of Ti and Al in weathering profiles, siliciclastic sediments and sedimentary rocks. J. Sediment. Res. 68, 448–455.
Yusoff, Z.M., Ngwenya, B.T., Parsons, I., 2013. Mobility and fractionation of REEs during deep weathering of geochemically contrasting granites in a tropical setting. Malaysia. Chem. Ceol. 349–350, 71–86.